Effects of additive manufacturing processes on part defects and properties: a classification review

Marc-Antoine de Pastre, Yann Quinsat, Claire Lartigue

Noname manuscript No.
(will be inserted by the editor)

Effects of additive manufacturing processes on part defects and properties: a classification review

Marc-Antoine de Pastre · Yann Quinsat · Claire Lartigue

the date of receipt and acceptance should be inserted later

Abstract *Additive manufacturing (AM) is an established manufacturing technology which allows for greater design freedom. Across the seven existing AM processes, we observe a variety of defects in printed parts, due to the different physical properties of each manufacturing process. This variety of defects complicates the design step without a clear overview of the deep interaction geometry-process-defect. The classification of these defects, which may be process- or machine-based, often raises methodological and terminological issues. In this paper, a review of AM general part defects using a process-based approach, is proposed. The aim of this paper is to provide the designer with a classification that would allow to make choices in the part design, by taking stock of the different defects affecting the resulting part considering the chosen process. For each process category defined in ISO/ASTM 52900, the main properties and defects of parts are reviewed and classified into four families: geometry and dimensions, surface quality, microstructure and mechanical properties. This review focuses in particular, on the process parameters which affect declined defects and properties allowing a relevant choice of the designer with respect to the process or the expected requirements of the part.*

Keywords Additive manufacturing processes; geometry and dimension; surface quality; microstructure; mechanical properties

List of abbreviations

Additive manufacturing process	
AM	Additive manufacturing
BJ	Binder jetting
CAD	Computer-aided-design
CAM	Computer-aided-manufacturing
CT	Computed tomography
DED	Directed energy deposition
EBPBF	Electron beam powder bed fusion
LPBF	Laser powder bed fusion
ME	Material extrusion
MJ	Material jetting
PBF	Powder bed fusion
SL	Sheet lamination
STL	Standard tessellation language
TO	Topology optimisation
VPP	Vat photo-polymerisation

Marc-Antoine de Pastre · Yann Quinsat · Claire Lartigue
LURPA, ENS Paris-Saclay, Université Paris-Saclay
91190 Gif-sur-Yvette, France
E-mail: marc-antoine.de_pastre@ens-paris-saclay.fr
E-mail: yann.quinsat@ens-paris-saclay.fr
E-mail: claire.lartigue@ens-paris-saclay.fr

1 Introduction

Additive manufacturing (AM) fundamentally revolutionises the way parts are manufactured, with a layer-by-layer approach, as opposed to traditional formative or subtractive manufacturing methods [1]. The groundbreaking nature of this technique allows for the production of complex geometries such as lattice structures [2,3] or topology optimised structures [4] that conventional manufacturing tools would be incapable of [5]. However, even though AM allows end-use part manufacturing in various applications, even high-valued once [5,6,7], resulting parts are not free from geometrical deviations in comparison to the nominal computer-aided-design (CAD) model. For the last three decades, there has been a massive deployment of AM machines and processes [8,9] shifting the focus to manufactured part characterisation in terms of part defects and the attending mechanical, electrical and acoustic properties. Indeed, as the material is built with process and geometry on symmetry, it is difficult to study one without the other. This part characterisation is deeply linked: the part geometry, the considered material, the manufacturing process and technology employed and even the observation technique which may impact the interpretation. As a result, defining a general defect and property classification compliant to any AM process is not an easy task. Literature shows that researchers rather focus on a specific AM process in order to find optimised machine parameters by conducting restrained-to-the-part defect analysis such as mechanical or microstructure studies. Defect categorisation has been performed for some AM processes [10,11,12,13,14] but not for all of them. Given that most AM processes have been established in relation to a precise material such as ceramic [15] or aluminium [11], it may not be adaptable for other materials such as polymer [16] or stainless steel [17]; raising the need for a synthesis for all AM processes, which does not exist to date. Additionally, a thoughtful design is mainly the result of the cooperation between the designer, the manufacturer and the metrologist. AM parts are challenging to produce as part material is produced simultaneously to its geometry, complicating the part defect and properties assessment within the process. Thus, an overview of all accessible defects considering a particular AM process, is an essential tool to clarify the designer's choice and to widen its interaction with the manufacturer and the metrologist. More precisely, an efficient design methodology can only be reached with the constant interaction performed between the designer, the manufacturer and the metrologist [18,19]. This communication allows to conciliate all design requirements, manufacturing and measuring constraints, leading to a customised, printable and measurable AM product [20]. In this paper, a defect and property classification review is proposed relying on AM process categories provided by ISO/ASTM 52900 [21]. More precisely, the aim of this paper is to provide a classification of defects and properties, suitable for all manufacturing processes based on the literature review. Most studies focus on defects and properties that affect the part ability to match its expected properties. Therefore, this review includes geometrical, surface or structural defects as well as mechanical properties such as strength or fatigue life. For each process category, the literature is synthesised through the proposed classification, giving a broader view of the most studied properties or defects by process category. Particular attention is paid to the process parameters influencing these defects and properties.

Section 2 presents the classification of general AM process categories as specified in ISO/ASTM 52900 [21]. This section also presents data processing steps from designing parts on dedicated CAD software until ready-to-use three-dimension (3D) printed parts. This section thus allows a clear identification of the possible source influencing defects and properties, and provides a common framework, relevant to all AM processes. In order to extend existing reviews to a general AM defect approach, section 3 highlights studied defects and properties according to these AM processes. When existing in the literature, process defect classifications are discussed. Otherwise, main works are presented and summarised then classified according to the proposed categorisation. Section 4 discusses trends raised in AM defect and property studies relative to each AM process category. This section proposes a synthesis comparisons of amount of works to identify needed works in specified classification families.

2 Overview of AM process categories

2.1 AM process categories and nomenclature

ISO/ASTM 52900 [21] provides an AM process classification declined according to seven AM process categories. These categories are defined in the following and illustrations are provided in Figure 1. In this paper, the referred geometrical axes are the axes described in Figure 1 for each AM process category.

- Binder jetting (BJ) - see Figure 1a. BJ consists in selectively projecting binder material in a powder bed successively spread to form a layer [21, 22,23,24]. BJ binds powder particles without external energy source except the binder projection and binder-drying lamp. As a consequence, resulting green parts are not subject to residual stresses which may cause resulting part deformations. However, without melting nor compression, binder jetted parts are more porous in comparison to powder bed fusion parts for example [23,25].
- Directed energy deposition (DED) - see Figure 1b. DED refers to the AM category in which metal is being melted while being deposited by focusing an energy source to the deposition site [21,22,26].

- Material extrusion (ME) - see Figure 1c. ME specifies the material selective deposition through a nozzle [1,21,27]. Polymer extrusion is seen widespread as the most general public accessible printing technology [27].
- Material jetting (MJ) - see Figure 1d. In the MJ category, parts are built by successively depositing photopolymer droplets which instantly turns into solid when submitted to ultraviolet lamps [1,21,28].
- Powder bed fusion (PBF) - see Figure 1e. PBF manufactured parts are obtained by selectively melting regions of powder successively spread in a building chamber [1,21,22]. The necessary amount of energy to fuse powder is provided either by laser technology [29] or by electron beam technology [30].
- Sheet lamination (SL) - see Figure 1f. SL process consists in stacking sheets of material which are bonded together and successively cut to form the 3D part [21,22].
- Vat photo-polymerisation (VPP) - see Figure 1g. In the VPP category, part is manufactured in a liquid photopolymer vat. Each layer is built by instantly transforming photopolymer to solid state using rastering ultraviolet laser [1,21,22,31].

For each of these process categories, different materials can be used. For example, PBF encompasses polymer PBF as well as metallic, ceramic or composite PBF. Adapted material to a specified AM process is summarised in Table 1.

AM process category	Adapted material
BJ	Ceramic Composite Metallic Polymer
DED	Metallic
ME	Ceramic[1] Polymer
MJ	Polymer
PBF	Ceramic Composite Metallic Polymer
SL	Ceramic Composite Metallic Polymer
VPP	Ceramic Composite Metallic Polymer

[1] Ceramics are not explicitly expressed as possible ME materials in ISO/ASTM 52900, but ceramics relevancy towards ME is shown in [32,33,34]

Table 1: Adapted materials for each specified AM process (according to ISO/ASTM 52900 [21])

However, each category dedicated to a given material can be declined according to the system technology under use. For instance, with the metallic PBF example, resulting parts can be obtained relying on laser technology or relying on electron beam melting technology. In other words, the methodology for classification of AM part properties is not an easy task as these classifications depend on the process category, the considered materials and the used technology.

2.2 From CAD to as-built parts

From original CAD to ready-to-use parts, a number of manufacturing steps have to be considered. These steps are detailed by Gibson *et al.* [1] and Thompson [35] which provide a generic framework which can be adapted to any AM process:

- Step 1: CAD. The part is created in a digital modelling software according to the designer specific intents.
- Step 2: Triangulation. The CAD file is converted into a triangulated mesh file format. The most commonly used file format is the standard tessellation language (STL). As an approximation of the CAD model, this conversion step introduces chordal errors as explained by Zha and Anand [36].
- Step 3: CAM Preparation. When the STL file is generated and oriented, support is to be generated (if required according to the process), then slicing the file and setting up the process parameters before sending the file to the machine.
- Step 4: File transfer to the AM machine. A machine-dependent code is then generated according to the considered AM process to build each of these layers.
- Step 5: Machine setup. The machine is initialised and process parameters such as laser power or drying time, are defined by the user.
- Step 6: Building. The part is built within the machine building chamber.
- Step 7: Removal and clean-up. Once the part is built, some processing steps may be required before extracting the part such as cooling timeouts of the building chamber or removal of excess built material. Then, the part can be removed from the building platform and cleaned up. The cleaning may be considered as the first post-processing step.
- Step 8: Post-processing. Some additional post-processing steps may be required such as removal of support structures, sintering, further curing or finishing and polishing. Post-processing requires user handling and may result in a lengthy task.
- Step 9: Application. The part is built, post-processed and ready to be used.

This list tends to provide a general pipeline from CAD to as-built part. Specific-to-the-process steps should be considered in order to improve the end-use part. For example, VPP should comprise a support definition step

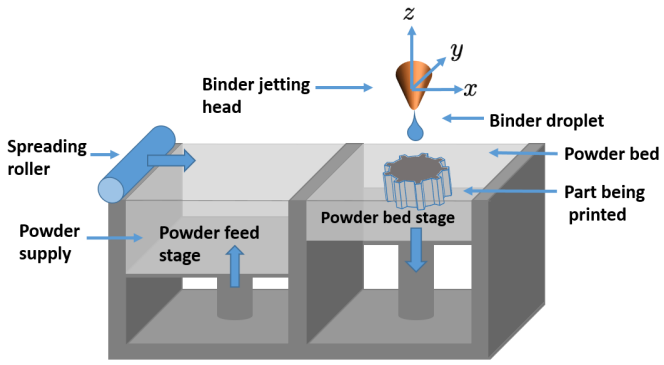

(a) Binder jetting (BJ)

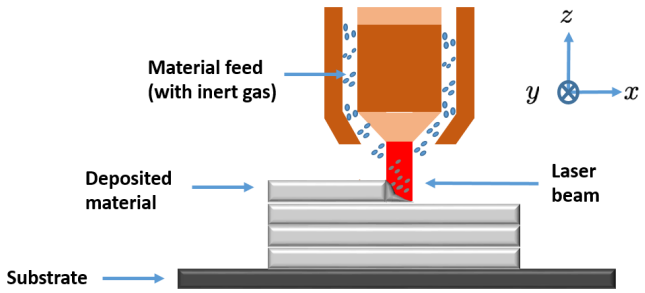

(b) Directed energy deposition (DED)

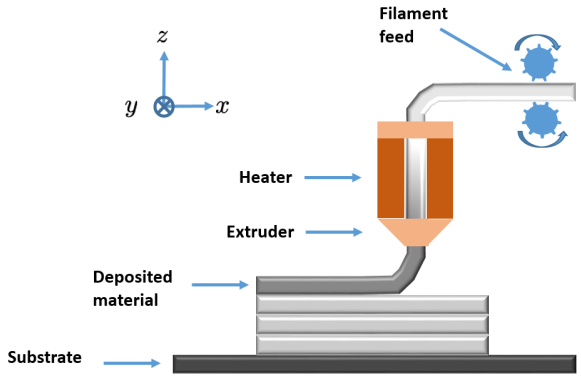

(c) Material extrusion (ME)

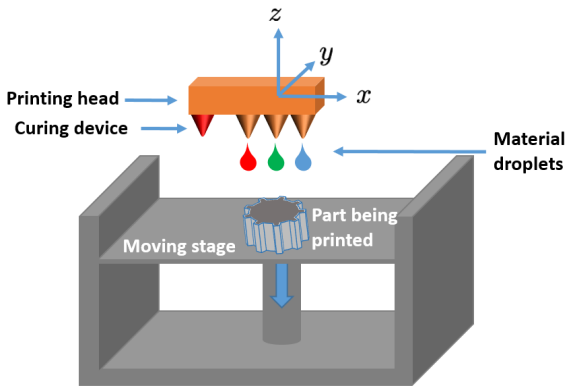

(d) Material jetting (MJ)

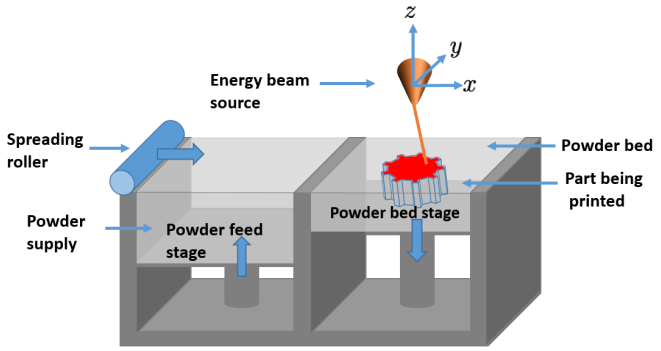

(e) Powder bed fusion (PBF)

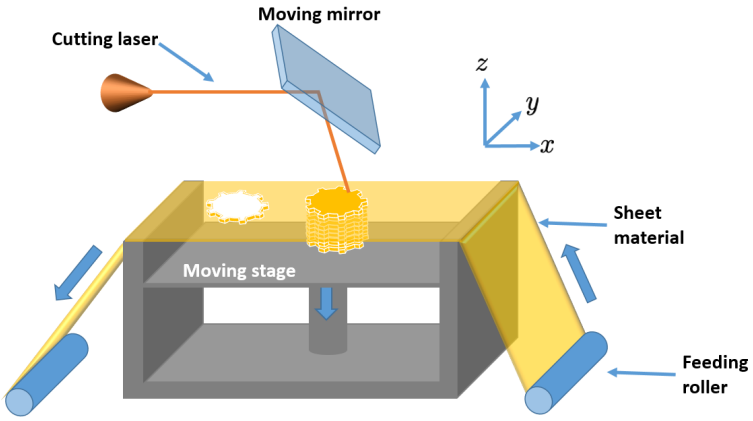

(f) Sheet lamination (SL)

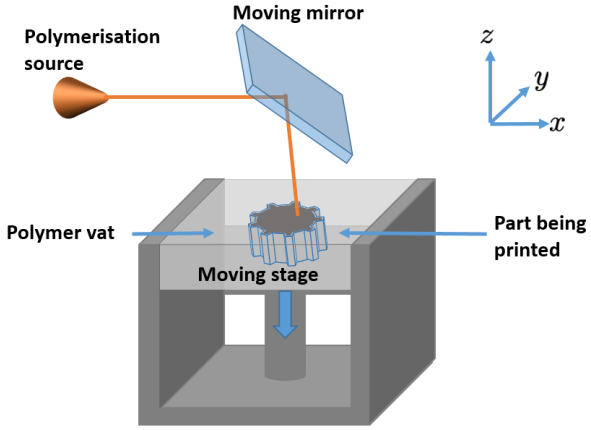

(g) Vat photo-polymerisation (VPP)

Fig. 1: Illustration of the seven ISO/ASTM 52900 [21] AM process categories

to increase the part manufacturability. This decomposition enables to better understand and identify in which step defects are most likely to occur. In this review, studied properties are mainly limited to steps 3, 4, 5 and 7.

3 General AM defect and property classification

AM defects and properties classification is multi-level where nomenclature, i.e. classification methodology, is of high importance for comprehensive sorting and comparison of AM part properties. As previously mentioned, defining a generic AM defect classification is not an easy task due to the multi-level origin of observed defects. Bourell *et al.* [37] proposed a list of defects affecting AM parts. More precisely, they referenced six types of defects relative to AM parts:

- Balling
- Porosity
- Cracks
- Distortion and delamination
- Poor surface finish
- Chemical degradation and oxidation

However, some of these defects may be linked. Balling defects, for instance, may result in an increased porosity or a part delamination [38] due to the discontinuity of melted pool for laser PBF process. Moreover, these defects are not sufficiently representative of the diversity of the AM defects encountered within a specific process. In other words, as defects are deeply linked to the considered AM process, we better think that defect and property classification should be conducted relative to a specific AM process category. In the following, the classification of part defects and properties is studied in the scope of a specific AM process category. Where existing, part defect and property classifications already established relative to a specified AM category are presented. A first analysis of the different classifications proposed in the literature highlights that it is possible to use a unique classification. Therefore, the following classification is proposed for each AM process category relying on a fourfold property decomposition:

- Geometry and dimensions
- Surface quality
- Microstructure
- Mechanical properties

Specific-to-process properties and defects are then declined and classified according to that common framework.

3.1 Binder jetting

BJ involves successive steps which possibly introduce defects of different natures. Indeed, for each layer, the binder is selectively projected onto the powder bed before being dried by heat lamp. In order to reinforce part properties, a sintering step is performed on the printed green part.

3.1.1 Geometry and dimensions

Geometrical and dimensional defects can be declined in a two-fold manner: dimensional inaccuracy of the printed part relative to the defined geometry and deformation effect such as shrinkage.

Dimensional inaccuracy

Dimensional inaccuracy is defined as the dimensional deviations between the printed part and its ideal defined geometry. The most obvious example of such deviations are chordal errors introduced during the file conversion step, whatever the considered AM process (see [36]). BJ allows the use of powder particles of 20 μm or less which is a main advantage in comparison to PBF for example [23]. Gaytan *et al.* [39] even performed a successive BJ printing of barium titanate using a particle size of 1 μm with a 30 μm layer thickness. However, Miyanaji *et al.* [40] highlighted that a larger metal particle size results in better dimensional accuracy.

Lores *et al.* [41] reviewed metal BJ recent developments. They showed that improvement of spreading rollers such as of ultrasonic vibrating or double smoothing mechanisms [42] reduce powder layer defects. Indeed, with a better powder spread, the layer density is increased which decreases risks of layer defects due to shear forces induced by the roller.

As investigated by Hsu and Lai [43], part accuracy also depends on the part location in the printing chamber. A better dimensional accuracy is obtained for part located near the powder supplier, which is the region firstly impacted by the roller [41].

Myanaji *et al.* [44] investigated printing speed effects on part accuracy. They highlighted a linear correlation between printing speed and part accuracy along the motion axis of the binder deposition head. Higher printing speeds mean lower part accuracy along the motion axis of the deposition head.

Binder material is dried by a heat lamp, which power is defined by the user. However, Miyanaji *et al.* [45] demonstrated that increased heat lamp power results in incomplete junction between particles for porcelain structures. Indeed, with a high heat lamp power, there is not enough time for the binder material to reach all the particles it is supposed to bind. This results in poor accuracy. Similarly, increased drying time results in weak bonds between particles which may lead to dimensional variations and loss of accuracy [41,45].

At the end of the printing process, binder jetted green parts are sintered to increase their properties such as density or mechanical strength (see dedicated sections). This sintering step is time-consuming and introduces distortions in the part (see deformation paragraph) [23]. As explained by Chavez *et al.* [46], final part accuracy

is highly dependent on the final grain size after the sintering step. Indeed, during sintering, particles are combined together, growing together to form the final grain size which affects final part accuracy.

Geometrical deformations

Geometrical deformations highlighted by this literature review reports shrinkage, which is the part contraction or expansion, as the main studied geometrical deformation defect. Relying on a Taguchi experiment, Chen and Zhao [47] showed that part shrinkage is highly dependent of binder drying time. With the same Taguchi approach, Wang and Zhao [48] highlighted that part shrinkage is higher along the building z direction, than along the x or y-axis.

Sintering step has also an important effect on part shrinkage. In BJ, powder is successively spread without packing force, resulting in low-density parts. In order to increase density and to improve mechanical properties, the sintering step is performed. During the sintering process, the part is submitted to shrinkage risk. Wang and Zhao [48] investigated sintering time, sintering temperature and temperature rise rates on shrinkage effects to find optimised values of these parameters via Taguchi experiments. Authors found that sintering time has the major effect on part shrinkage along all axes. Sintering time and temperature rise rate effects depend on the considered axis: temperature rise rate has more effect on the z-axis shrinkage and sintering time affects more the x-axis shrinkage.

3.1.2 Surface quality

In this literature review, surface quality is mainly referred to as part surface roughness, evaluated by ISO 4287 average roughness R_a value [49] converted into a signal-to-noise ratio study [47]. Chen and Zhao identified that roughness depends on the layer thickness: surface roughness decreases with thinner layer thickness.

Saturation level is believed to impact surface quality. Printing saturation level defines the amount of binder deposited relative to the powder bed [41,47]. As explained by Lores *et al.* [41], a lower saturation level means that binder has not been sufficiently deposited to bind all particles it is supposed to. This results in particle detachment or separation leading to surface quality decrease. Conversely, too high saturation levels increase the number of attached particles and results in excessively deposited powder binder which affects surface quality.

Furthermore, Miyanaji *et al.* [40] also argued that smaller particle sizes lead to improve surface finish. Do *et al.* [50] noticed a small diminution of the R_a values after the sintering step.

3.1.3 Microstructure

In the BJ scope, microstructure is referred to as porosity or powder density. Asadi-Eydivand *et al.* [51] identified that BJ significant parameters affecting the resulting green part porosity are part orientation, layer thickness and delay time needed to spread the next layer of powder.

Particle shape is of great influence on the green part density. As shown by Mostafei *et al.* [52], particle morphology impacts part density: spherical particle-based parts are denser than irregular particle shape based parts.

Binder jetted parts have low density because of the spread of powder layers with minimum roller efforts [41]. As a result, a densification step by sintering is needed when increased mechanical properties are expected. Using computed tomography (CT), Zhu *et al.* [53] illustrated the pore evolution during sintering. Evolution of pores according to sintering temperature is also described by Do *et al.* [50]. Micrographs of bore-based samples for different sintering temperatures are shown in Figure 2. Indeed, as explained by Chavez *et al.* [46], density evolution during sintering depends on sintering temperature. The higher the sintering temperature, the denser resulting part. However, longer sintering times increase the risk of part shrinkage and warping [41].

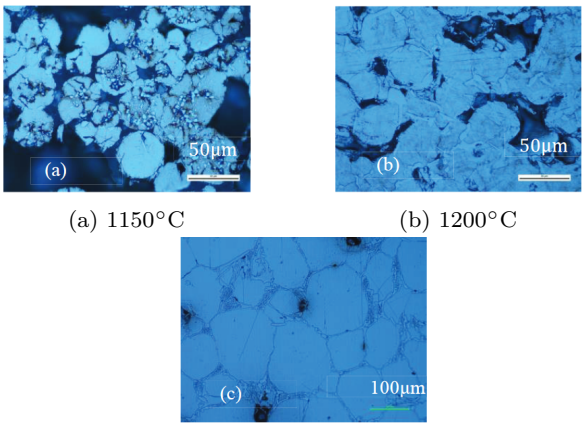

(a) 1150°C (b) 1200°C

(c) 1250°C

Fig. 2: Microstructure of bore-based samples for different sintering temperatures shown in [50]

3.1.4 Mechanical properties

In BJ processes, mechanical properties of printed parts have been widely investigated. In this review, such properties are summarised according to mechanical strength and cracks.

Mechanical strength

Chumnanklang *et al.* [54] argued that mechanical strength of bioceramic green parts (before sintering) is increased with the increase of pre-coated particle size. However, for metallic powder, Miyanaji *et al.* [40] found that a smaller particle size would increase mechanical strength. Authors further investigated the effect of binder saturation levels on the resulting strength. Their exper-

iments revealed that mechanical strength is increased with saturation levels. This result is shared with Chavez *et al.* [46] whose experimental observations revealed increased elastic modulus with increased saturation levels. Miyanaji *et al.* [45] found that increasing binder saturation levels from 50% to 75% increased the part strength by 50% for porcelain structures. Miyanaji *et al.* [44] studied the effects of printing speed on part strength. With increased printing speed, binder saturation levels decrease leading to decreased mechanical strength, according to [43,46,54].
Doyle *et al.* [55] investigated the effect of layer thickness and part orientation on the resulting stainless steel and bronze part strength. The authors found that layer thickness has more impact on part strength than orientation. They also identified that part density is of huge influence on mechanical properties. Indeed, the sintering step allows mechanical properties to be increased by densification of the green part. This point is also demonstrated by Chumnanklang *et al.* [54] who found that mechanical properties were increased after the sintering of the green binder-jetted part.

Cracks
Cracks occur when material is submitted to high shear efforts. Even though BJ successively spreads powder without packing forces, initial layers may be displaced due to increased roller shear efforts, resulting in crack formations [41]. Furthermore, cracks in the resulting layer are affected by the powder distribution strategy: too much spread powder raises these shear forces while risking crack formation. As explained by Lores *et al.* [41], excessive dried layers are prone to cracking due to the shear efforts induced by the roller spreading the next layer.

3.1.5 Electrical properties

It is worth mentioning works performed on BJ electrical properties in this classification review. Chavez *et al.* [46] investigated evolution of the ceramic dielectric constant according to sintering temperature. Results showed that increased sintering temperatures lead to increased values of dielectric constants. Authors additionally studied the impact of part orientations on piezoelectric properties highlighting a correlation between mechanical and piezoelectric properties.

3.1.6 Summary

Table 3 summarises the BJ property review and influence parameters outlined in the previous section.

3.2 Directed energy deposition

DED is a complex process involving many physical principles, the monitoring of which is not an easy task. DED processes are commonly categorised into: laser-based DED, arc-based DED, electron beam DED depending on the kind of energy used. Significant efforts have been made to develop in-situ process monitoring and dedicated property identification algorithms. For example, Chabot *et al.* [56] recently highlighted ultrasonic testing relevancy for in-situ monitoring of defects whose size comprises 0.6 mm to 1 mm. Further works and developments are reviewed by Everton *et al.* [57] and Kim *et al.* [58].

3.2.1 Geometry and dimensions

Geometrical and dimensional defects are mainly referred to as dimensional inaccuracies. Geometrical deformations of the printed part are less studied and mainly described as part shrinkage.

Dimensional inaccuracy
As explained by Bi *et al.* [59], size and temperature of the melt pool have a direct influence on the dimensional accuracy of the printed part. Authors particularly highlighted edge effects in the clad deposition procedure with a constant laser power. More precisely, edge effects due to cooling rate variations and acceleration setups impact wall thickness or edge clads for example. Typically, DED parts printed with constant laser power present increased edge heights. Authors then proposed a path-dependent laser power to decrease such inaccuracies. Masaylo *et al.* [60] described low deposition rate effects on the final geometry which tends to be heightened. This effect is more pronounced where the deposition head changes its motion direction. Adopting a unidirectional strategy may improve the part geometry. Atwood *et al.* [61] expressed that decreasing layer thickness results in a better part accuracy. Moreover, their measurements revealed better accuracy in the x-y plane than along the z-axis.
In wire-based DED, Heralić *et al.* [62] proposed a z-axis compensation controller in order to correct flatness deviations while building the part. In other words, a 3D scanner is integrated within the building cell and compensation of the layer height is performed by controlling the wire-feed rate. Similar works were performed by Chabot *et al.* [63] involving in-situ ultrasonic sensor to correct deposition head vertical position and improve dimensional accuracy of the printed parts.

Geometrical deformation
Geometrical deformation is mainly referred to as shrinkage notably by Bi *et al.* [59] who defined DED part shrinkage. Indeed, clads located in the edges of the part are cooled in a faster way than clads in the middle of the part. As a result, the part outside wall is prone to shrinkage directed towards the inside of the part due to that high cooling rate ratio.

3.2.2 Surface quality

Surface quality in the DED field of study is referred to as evaluation of R_a average roughness parameter.

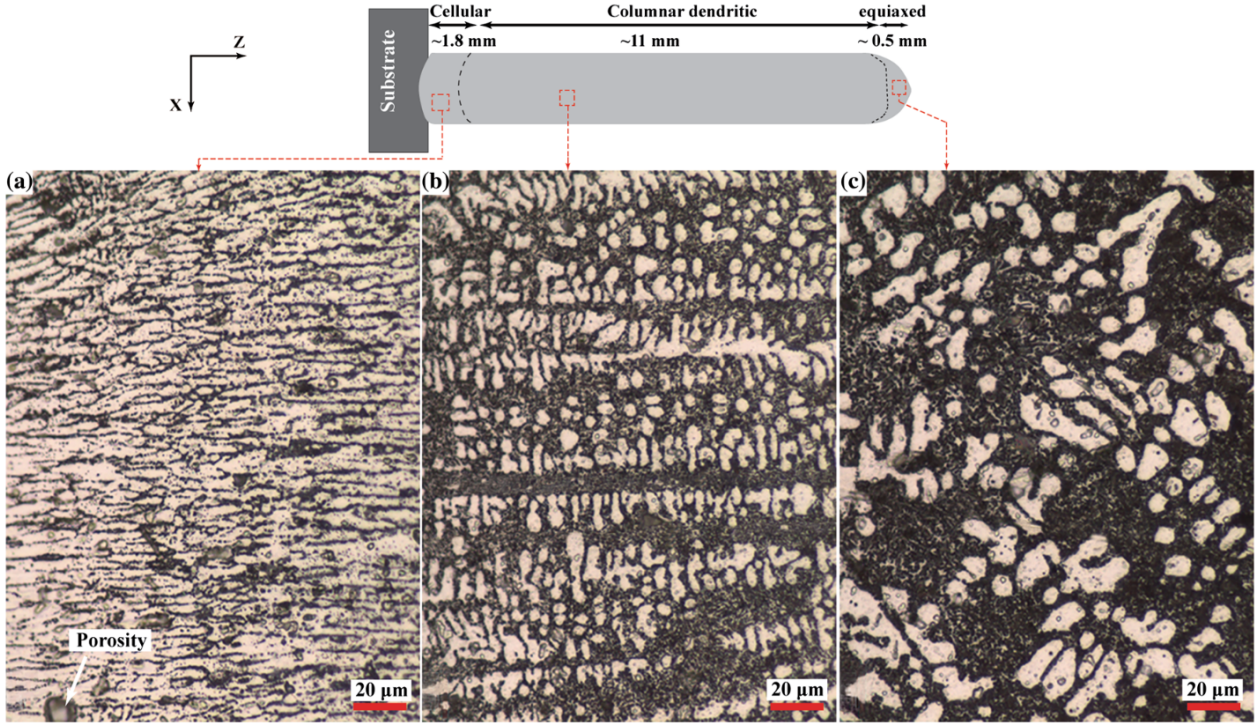

Fig. 3: Description of DED AlSi10Mg alloy morphology evolution along the building direction provided by Javidani *et al.* [26]. Morphology evolves from the substrate (left side) to the last deposited layers (right side)

Atwood *et al.* [61] reckoned that DED parts are naturally rough, with established R_a values reaching about 5.08 μm to 7.62 μm (original inch values have been converted). Toyserkani and Khajepour [64] proposed a method to evaluate the clad surface roughness, by application of a pattern recognition procedure which finds back clad height fluctuation from image acquisition.

3.2.3 Microstructure

In the DED process, microstructure studies focus on different kinds of defects. These defects are summarised according to morphology, oxide inclusion and porosity.

Morphology

The part morphology and microstructure grain orientations are the most studied DED defects. Grain structure orientation is widely examined in the literature. Grain texture orientations depend on many parameters notably temperature gradients or cooling rates [65]. More precisely, grain morphology has been observed for titanium-based alloys [66,67,68], for aluminium alloys [26], nickel-based alloys [69], stainless steel-based alloys [70,71] and cobalt-based alloys [72]. These works highlighted a grain morphology modification of the printed material. Indeed, as shown by Javidani *et al.* [26] for aluminium alloys, the substrate material, i.e. the material on which the first layer is printed, impacts the solidification of the first deposited clads. On initial layers, solidified features appear as cellular features. As height increases, so does the distance of deposited material from the substrate. These features are progressively turned into dendritic columnar with an orientation depending on the heat release flow direction. On the final layers, the observed part presents equiaxed dendritic solidified features. Such a description is shown in Figure 3. Similar observations were conducted for other kinds of materials. Saboori *et al.* [67] outlined the solidified feature modification with height for titanium parts as depending on the temperature gradients and solidification rates. High temperature gradients combined with low solidification rates result in columnar features. Conversely, low temperature gradients combined with high solidification rates result in equiaxed grains. Similar conclusions were drawn by Shamsaei *et al.* [65] based on Selcuk's works [73].

Saboori *et al.* [67] also summarised different works investigating the layer-by-layer process impact on the solidified feature structures and their effects relative to the entire part (see for example Liu *et al.* [74]).

Zhang *et al.* [72] investigated steel DED process for repairing damaged parts made of a different material. Authors particularly focused on feature discontinuity on the interface between original and deposited materials.

Oxide inclusion

Oxide inclusion defects are described by Masaylo *et al.* [60] specifically for stainless steel alloys with a high chromium level. Oxide inclusions are small intern spatters composed of oxygen and chromium created by oxygen entrapped in the powder, powder moisture or oxygen in the deposition working chamber [60]. Authors provide solutions to minimise oxide inclusion such as introducing a preliminary powder drying step or using protective means while printing.

Porosity
In the DED process scope, there are two kinds of porosities [57]:

- trapped gas during the solidification process.
- interlayer porosity.

Trapped gas has been studied by Zhang *et al.* [75] by observing evolution of trapped gas in the melt pool. Authors described the bubble formation and evolution, and the impact on surface porosity whether the bubble explodes on the surface or is retained in the melt pool. More precisely, they asserted the competition between solidification velocity and gas bubble release due to the growth rates of the bubble inside pressure.
Interlayer porosity is caused by the lack of fusion between layers [57], incorrect laser power, robot speed or powder amount deposited [60] resulting in voids being partially filled with gas or unmelted powder spatters [60].
DED porosity was estimated by Javidani *et al.* [26] using volumetric measurements performed by Archimède methodology. Gaja and Liou [76] used an acoustic emission sensor, i.e. a piezoelectric transducer, to identify gas pores.

3.2.4 Mechanical properties

Main DED works on mechanical properties reveal five topics relative to associated properties: strength, cracks, hardness, residual stresses and fatigue behaviour.

Strength
Shamsaei *et al.* [65] and Saboori *et al.* [67] reported works performed on resulting mechanical strength of parts printed by the DED process. They reported higher tensile properties along the x-axis. Indeed, as described by the authors, the x direction, which is the deposition head direction provides higher cooling rates as heat is evacuated by natural metal conduction. Such samples have a thinner microstructure compatible with higher tensile strength [65,67].
In the repair application for aluminium-based alloys described by Zhang *et al.* [72], authors found a DED-repaired part presenting an increased tensile strength in comparison to the original part. However, authors outlined the change of mechanical behaviour: the repaired part is less ductile with almost no yielding zone whereas the original part was much more ductile presenting wider yielding zone. Rauch *et al.* [77] found similar results in the same repairing application for titanium-based alloys, highlighting decreased ductility of repaired parts.

Cracks
With microstructure, crack formation is the second most studied defect in DED works reviewed in this paper. According to Everton *et al.* [57], crack formation results in the difference in the material thermal expansion coefficients during the printed process resulting in shear stress in the material. Experimentally, acoustic techniques or ultrasonic techniques adapted to the DED process [78,79] have been shown to successfully identify crack formations [76,80]. Wang *et al.* [80] showed for example that DED crack formations increased with material thickness and with increased cooling rates.

Hardness
As reviewed by Shamsaei *et al.* [65] micro-hardness values measured from a DED part differ, depending on the investigated region. Authors assumed the cooling rate to be responsible for this observation. This statement is detailed by Javidani *et al.* [26] who showed that hardness of aluminium alloys highly depends of the microstructure feature. Indeed, dendritic solidified features showed lower Vickers hardness values than the cellular morphology. Bi *et al.* [59] used Vickers hardness measurements to validate their path-dependent process control which modulates laser power intensity according to the followed path. In the repair context detailed by Zhang *et al.* [72], Cobalt-based alloys deposits are found to have higher Vickers hardness than the steel substrate. Such a high value is explained by the rapid cooling rate at the substrate interface and the fine obtained microstructure.

Residual stresses
Shamsaei *et al.* [65] also reviewed main works on residual stresses. Rangaswamy *et al.* [81] used neutron diffraction to identify residual stresses in DED parts. Authors showed that residual stresses are uniaxial and aligned with the deposition head motion. Residual stresses are shown as compressive in the middle of the sample and more tensile near the edges [81]. Along the z-axis, residual stresses are mainly compressive near the substrate. These compressive stresses slowly decrease with height and are then substituted by tensile stresses until the top surface [65]. However, in order to reduce residual stresses, local thermal gradients should be decreased. In order to impact thermal gradients, users may optimise process parameters or apply heating of the substrate during the process [65]. The chosen path strategy [82] to maintain thermal gradients substantially constant during the process remains under question.

Fatigue
Fatigue properties, fatigue models and fatigue crack formations of DED parts are reviewed by Shamsaei *et al.* [65]. Atwood *et al.* [61] established that DED parts have increased fatigue properties. Indeed, as shown by Razavi *et al.* [66], DED parts underwent a higher number of cycles before cracking than wrought equivalent part. As explained by the authors, DED parts present finer grain sizes resulting in a better fatigue behaviour. Bandyopadhyay *et al.* [83] investigated the effect of deposition orientation on Ti6Al4V fatigue performance. They showed that vertical tested parts have an increased interlayer porosity that weakens their fatigue performances in comparison with horizontal parts.

3.2.5 Summary

Table 4 summarises the DED property review and the influence parameters outlined in the previous section.

3.3 Material extrusion

ME defects have been reviewed and classified in several papers. Penumakala *et al.* [84] recently proposed a thermoplastic polymer composite-based review. Their works particularly showed how thermoplastic composites are being reinforced in order to improve the printed part mechanical properties, with regard to the part application requirements. However, different defect classifications have been proposed according to literature. In 1996, Agarwala *et al.* [85] proposed a binary classification considering that defects could be divided in surface or internal defects. More precisely surface defects encompass support staircase effects, curve approximation errors, top and bottom surface aspects, defects due to the deposition delay when head motion starts or stops and support structure removal effect on part quality. On the other hand, internal defects have different origins such as:

- voids generated by abrupt movement changes of the deposition head.
- voids generated when turning or by bonding weakness between adjacent paths due to increased cooling time with a long path.
- filament slippage occurring in the filament feeding system resulting in a lack of deposited material and weak bonding.
- a non-uniform deposited filament diameter.

In their paper, authors also investigate influence factors which can reduce these observed defects [85].

In 2018, Papazetis and Vosniakos [86] conducted Taguchi experiments linked to an artificial neural network evaluating the influence of layer thickness, material flow, deposition head velocity and plane orientation in the resulting part shape conformity to its CAD model. As described by the authors, they identified defects as:

- 'Deformed edges'
- 'Under-extrusions'
- 'Weak fibre bonding'
- 'Base bulging' which can be defined as the crushing of the first layers

These defects are shown in Figure 4.

Wickramasinghe *et al.* [13] conducted a comprehensive review on fibre-reinforced material extruded parts. They outlined the diversity of works performed to characterise mechanical properties, part defects, process and surface treatments regarding ME parts. In depth, they listed part defects integrating fibre-reinforced ME parts as follows:

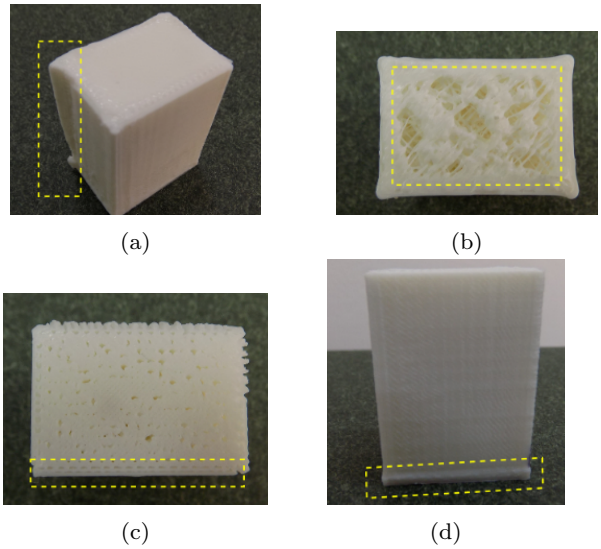

Fig. 4: Illustration of ME defects defined by Papazetis and Vosniakos [86]: (a) deformed edges; (b) under extrusion; (c) weak fibre bonding; (d) base bulging

- Shape distortion, a result of residual stresses trapped in the printed part due to non-uniform temperature gradients. Shape distortion is mainly expressed as shrinkage. Shrinkage affects part by layer delamination and warping (also referred to as curling in the literature). Authors note the advantage to adopt an adhesive printing platform to weaken warping effects on extruded parts.
- Micro-voids between fibre and polymer.
- Uneven fibre distribution in the fibre-reinforced filament.
- Poor bonding of fibre introduced inside filaments.
- Surface roughness mainly affected by staircase effect of layer deposition.

In the interest of consistency with other AM process categories, Table 5 translates these reviewed defects into the proposed defect and property classification. Although this review mainly focuses on mechanical engineering parts, it is worth mentioning major works performed in the civil engineering field by the development of concrete extrusion processes [87,88]. These works do not lead to the same level of defects as considered in this paper but mechanical aspects of resulting application should be outlined.

3.4 Material jetting

MJ process has the particular advantage of printing multi-material parts, raising the interest of various actors such as biological engineering or electrical circuit engineering [58].

3.4.1 Geometry and dimensions

Geometrical and dimensional MJ defects may be classified by dimensional inaccuracy and geometrical deformation of the printed part.

Dimensional inaccuracy

Vaezi *et al.* [89] explained that the final part geometry being printed using MJ is highly dependent on the shape of the droplets involved in the printing process. Indeed, by reviewing main parameters affecting part quality, authors identified that the deposited droplet shape influences the resulting part precision and accuracy. Similarly, according to Tourloukis *et al.* [90], the MJ printer performance depends on its ability to control the droplet ejection, deposition and curing mechanisms. More precisely, a wide understanding of the process is required to significantly increase the printed part accuracy, by selecting appropriate printing parameters. Sturm *et al.* [91] developed an in-situ impedance-based measurement methodology to monitor the part quality whilst printing. In other words, authors used electromechanical impedance measurements to track the built geometry. That monitoring enables to induce in-process changes and to minimise part deviations relative to the defined geometry.

Geometrical deformation

MJ deformation is mainly referred to as part shrinkage due to residual stresses accumulated within the part. In the biomaterial field, Ebert *et al.* [92] noticed a part volumetric isotropic shrinkage about 20%. Koshkoo *et al.* [93] investigated part thickness and build orientation effects on the induced distortion. Distortion is, indeed,mainly the resulting effect of internal residual stresses. These residual stresses are generated when material is deposited along previously cured deposited material, resulting in a thermal gradient heterogeneity. Koshkoo *et al.* [93] printed two sets of 100×10 (mm^2) samples with different thicknesses, ranging from $1mm$ to $6mm$. One set is printed along the x-axis, and the second one along the y-axis. Height elevations were acquired with a profilometer. Results showed that thin parts tend towards waving distortion shapes whereas thicker parts tend to reverse coil distortion shapes. Moreover, distortion effect is shown to be more important for part printed along the x-axis, i.e. the longer rastering distance in the deposition head motion. Indeed, along the x-axis, a significant delay applies between two adjacent paths. On the next path, material is then adjacently deposited to an already cured material. This delay increases the thermal gradient intensity resulting in residual stresses.

3.4.2 Surface quality

MJ works on surface quality concern roughness evaluation. Cazón *et al.* [94] as well as Pugalendhi *et al.* [95] identified that the glossy surface finish drastically improved the surface roughness. However, glossy surface finish may be detrimental to the thin walls and may not be recommended for part including thin features, with authors further arguing that parts positioned in the x-y plane have lower roughness values.

Kechagias and Maropoulos [96] investigated the impact of part tilt orientation (which corresponds to part inclination) on the resulting surface roughness. They showed that lowest roughness values were obtained for 0° tilt angle whereas maximum roughness was obtained for 90° tilt angle. In a deeper analysis, Kumar and Saravan Kumar [97] used matt and glossy samples made of regularly tilted platens to incrementally cover all building tilt orientations. They used a typical truncheon artefact which is shown in Figure 5, and which has been formerly described in [98,99,100].

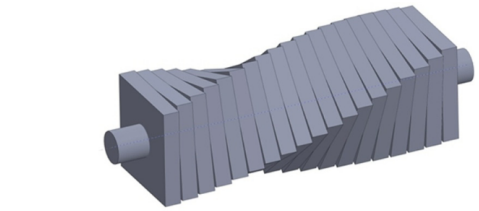

(a)

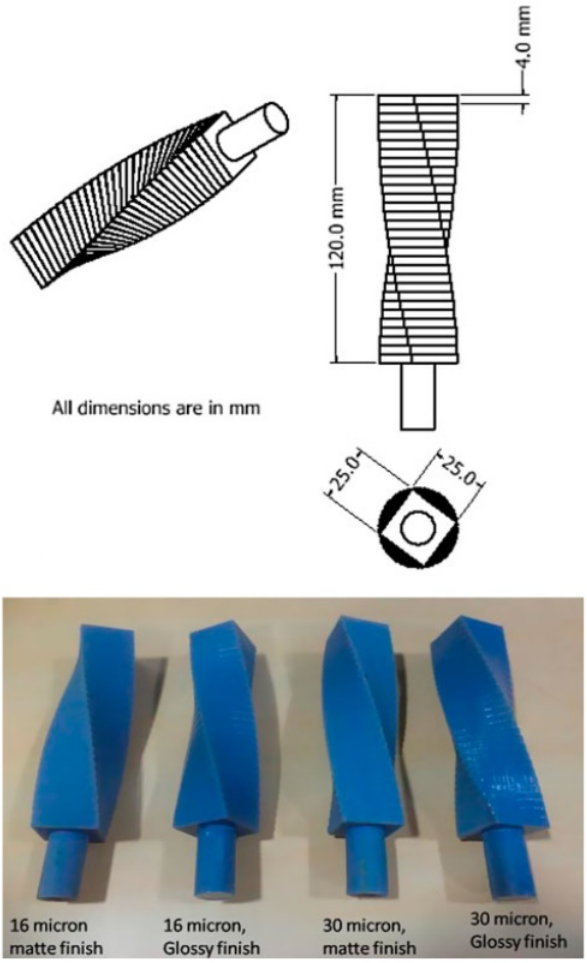

(b)

Fig. 5: Illustration of the truncheon artefact: (a) CAD definition (Udroiu *et al.* [101]); (b) used samples by Kumar and Saravan Kumar [97]

Authors used predictive drop deposition and curing modellings to predict surface roughness. They could compare predicted roughness values with measured ones on all the surfaces comprised in their specified sam-

ples. As Kechagias and Maropoulos [96], Kumar and Saravan Kumar [97] showed that surface roughness increased from 0° to 90° (i.e. the part top-facing surface), and further decreased from 90° to 180° (i.e. the down-facing surface). The layer thickness does not significantly influence the resulting surface roughness. As explained by the authors, the staircase effect is of very little influence for layer thickness considered in MJ [97, 102].
Udroiu *et al.* [101] extended Kumar and Saravan Kumar's works [97] by investigating effects of tilt angle, finish type and part orientation within the printing area on the part roughness. Their designed artefact, similar to Kumar and Saravan Kumar's [97], has been placed in different orientations in the x-y plane. Surface roughness values of each printed part was compared to the expected theoretical values. As a result, the glossy part perpendicular to the head motion direction results in the lowest roughness values.

3.4.3 Microstructure

Microstructure has not been studied in the same depth that aforementioned defects. Moore and Williams [103] observed voids in MJ materials. Authors assumed these voids to have a drastic impact on the part fatigue life.

3.4.4 Mechanical properties

In the scope of MJ mechanical properties, the proposed classification is strength, fatigue and ageing effects on mechanical properties.

Strength
Cazón *et al.* [94] investigated the part orientation and the surface finishing effect on the mechanical strength by printing differently oriented and finished parts. Authors showed that matt parts have lower elastic modulus than glossy parts. Moreover, parts printed along the x-axis, which is the main motion axis of the head, have the highest elastic modulus. Resulting ductility also depends on the printing direction as parts printed in the x-y plane are more ductile than the z-axis printed parts. Bass *et al.* [104] found the same x-axis condition when comparing orientation effect on mechanical properties for different rigid and elastic MJ parts. Authors identified that parts being printed in the z-axis direction have the weakest mechanical strength.
Pugalendhi *et al.* [95] processed MJ parts with different printing conditions ending up with glossy or matt surface finish for two printing strategies: high quality or high-speed printing. By conducting tensile, flexion and hardness evaluations, authors found that the 'high-speed' glossy part has better mechanical properties. Indeed, this part shows higher values than other studied samples in terms of tensile strength, elongation at break, flexural strength and shore hardness.
Vu *et al.* [105] characterised printing orientation on multi-material interfaces by evaluating and investigating their mechanical properties. More precisely, the part orientation of multi-material sandwich is shown to have an important impact on the material fracture resistance. As shown by the authors, multi-material parts where 'sandwich' layers are printed in x-y plane, exhibited better fracture resistance properties.

Fatigue
Moore and Williams [103] found a relation between elongation and fatigue cycles for MJ parts. Authors showed that glossy surface finish considerably improved fatigue life properties up to 37% longer than non-glossy part fatigue life.
Kaweesa and Meisel [106] focused on the multi-material aspect of MJ parts on fatigue life properties. Indeed, multi-material MJ parts tend to break along the material interface. Thus, authors designed and printed gradient-based samples where transition between materials relies on a gradual material change. Their works emphasised the gradient-based transition between materials as being of influence on the resulting fatigue life properties. Moreover, parts with shorter transition length lead to a higher fatigue life.

Ageing
Bass *et al.* [104] conducted a study on the ageing effect on MJ part mechanical properties. More precisely, for ten weeks, they weekly evaluated ultimate tensile strength and elastic modulus of two sets of parts printed in the x-axis (which is the axis leading to the best mechanical strength). The first set has been regularly exposed to fluorescent light, and the other set has been conserved in an opaque box, with no light exposure. Results showed that ageing increased mechanical ultimate tensile strength, and decreased elongation at break. However, as argued by the authors, conditions of light exposure do not seem to affect MJ part mechanical properties.

3.4.5 Summary

Table 6 summarises the MJ property review and the influence parameters outlined in the previous section.

3.5 Powder bed fusion

Regarding literature, PBF is one of the most and diversely studied. PBF part properties and defects have already been reviewed by several authors. Indeed, all of these works primarily distinct the process technology used to melt powder bed: laser or electron beam. On a second level, reviews focus on a specific material used in the process. The aim of this section is then to discuss and to compare existing reviews in order to extend these works to a general overview.
Malekipour and El-Mounayri [10] precisely studied laser PBF (LPBF) defects highlighting the influential parameters for each of the outlined defects. Their defect classification is summarised in Table 7. Similarly, Galy *et al.* [11] provided the defect typology performed

for aluminium alloys produced by LPBF. In a deeper analysis, they declined a fourfold classification of aluminium alloys LPBF defects as porosity, hot-cracking, anisotropy and surface quality by developing cause trees to track back the influential main parameters.
Vo *et al.* [107] provided a defect classification for electron beam PBF (EBPBF). Their classification is very similar to Malekipour and El-Mounayri's [10] apart from the geometrical and dimensional point. Whereas geometrical and dimensional defects are declined as form and size defects by Malekipour and El-Mounayri [10] for LPBF, Vo *et al.* [107] rather declined them as geometrical inaccuracy and geometrical deformation for EBPBF. Geometrical inaccuracy encompasses for example staircase effect or machine positioning errors. Geometrical deformation refers to warping, loss of edge and loss of thickness occurring during the printing process [107]. These defects are illustrated in Figure 6. Both classifications have inspired the classification methodology presented in this review.

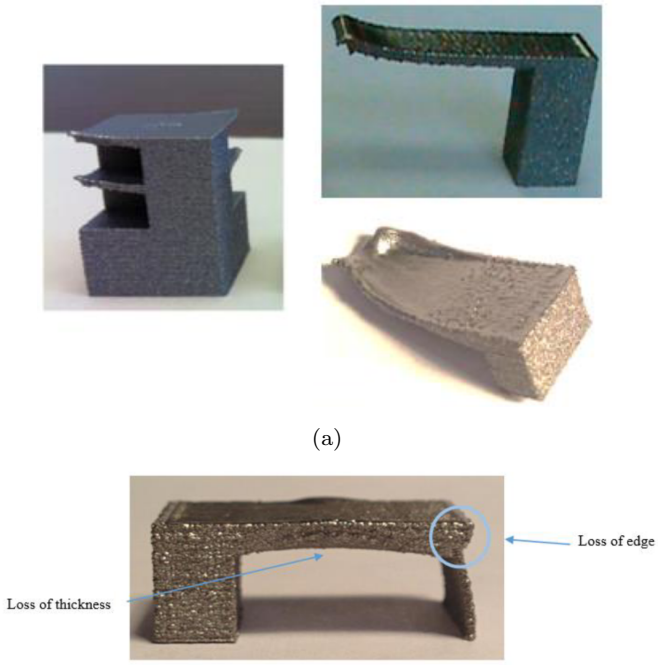

(a)

(b)

Fig. 6: Illustration of geometrical deformations described by Vo *et al.* [107] for EBPBF: (a) warping; (b) loss of edge and loss of thickness

3.6 Sheet lamination

Although SL allows the production of metal-based [108], ceramic-based [109], polymer-based [110] or paper-based parts [111], SL process remains the same. Sheets of materials are successively rolled, and layer outlines are cut by a laser. Then, a roller bonds the current layer to the previous one. SL is then adapted to produce composite parts and heterogeneous material by adding prefabricated material between layers [112]. For polymers, ceramics or paper-based materials, the heated roller activates thermo-active glue spread over the previous layer. For metal-based materials, bonding is mainly performed by ultrasonic waves emitted by a sonotrode roller resulting in the layer fusing by vibration and friction response of the metal sheet.

3.6.1 Geometry and dimensions

Kechagias [113] investigated process parameter effects on the resulting paper part dimensional accuracy using Taguchi experiments on typical cubic samples. Results showed that dimensional accuracy is significantly different along the x-axis or along the y-axis. Heater rolling speed is identified as the main parameter influencing the part dimensional accuracy in the x-y plane. Vertical dimensional accuracy depends on moisture absorption, layer thickness and material compaction. Pilipović *et al.* [110] focused on the influence of the part position in the printing machine on geometrical deviations and mechanical properties. Authors designed prismatic test parts built by three different methods: layer stacking along the part height, layer stacking along the part width, and layer stacking along the part length. These three layer stacking configurations are shown in Figure 7a. Results showed that parts printed along the part length have the lowest geometrical deviations. Authors also explain the highest vertical geometrical deviations by thick polymer film width and bonding glue effects. With metallic SL, precise laser cut combined with sonotrode roller bonding technique offers great geometrical accuracy in x or y directions. However, accuracy along the z-axis is harder to control due to the layer thickness modification while sheets are being compressed and bonded [108].

3.6.2 Surface quality

In SL, surface quality defects are described as surface roughness. In their works, Pilipović *et al.* [110] found that the top surface of the polymer part printed in the x-y plane has the lowest R_a value. Indeed, in that layout, top surface is made of the last deposited and cut polymer film.
Kechagias [111] performed a design of experiment approach to identify parameters of influence among layer thickness, heated roller temperature and speed, platform retract, laser speed, feeder speed and platform speed, on the resulting part roughness evaluated along the z-axis. Results showed that the R_a value evaluated along the z-axis mainly depends on the heated roller temperature, the layer thickness and the laser speed.
Chryssolouris *et al.* [114] developed R_a semi-empirical prediction model relying on influential main parameters: layer thickness, heated roller temperature and speed, and platform retract. Paul and Voorakarnam [115] developed a roughness quantification model depending on layer thickness and surface orientation us-

ing a parabolic curve surface representation. Contrary to Chryssolouris *et al.* [114], Paul and Voorakarnam [115] made the distinction between up-facing and down-facing roughness in their model description. They assessed their model by evaluating R_a values evaluated for different tilt angles with different layer thickness highlighting a good agreement between predicted and measured R_a values.

Similarly, Ahn *et al.* [116] used Paul and Voorakarnam's parabolic curve predictive roughness model [115]. In order to validate their model, authors evaluated R_a values in the up-facing part, i.e. in the range 0° to 180°, using a paper test part comprising regularly tilted planes. This sample enabled to investigate the influence of layer thickness and penetration depth of laser cut. Results showed that surface roughness decreases in the up-facing part from 0° to 90°, and increased in the down-facing part from 90° to 180°, as predicted by the model. Moreover, increased layer thickness tends to increase resulting part roughness. Authors also outlined the penetration depth effect of the cut laser in the resulting roughness. However, penetration depth has a minor effect in comparison with the layer thickness.

3.6.3 Mechanical properties

Tensile strength

Chryssolouris *et al.* [117] investigated influence of process parameters, such as layer thickness, heated roller speed and the temperature or platform retract, on the resulting paper part strength. Authors relied on a statistical design experiment analysis (Taguchi methodologies) and identified layer thickness as the main parameter influencing the resulting tensile strength. With increased layer thickness, the produced part has an increased tensile strength. Indeed, as explained by the authors, low values of layer thickness induce more layers and thus more glue to bond layers. As a result, as bonding glue has lower mechanical strength than paper, the wider glue layers, the less resistant resulting part. However, in polymer SL, Zhang and Wang [118] showed the impact of time and temperature used to bond layers. They highlighted that, increasing compression time or bonding strength increases interdiffusion between layers, and thus the resulting part shear strength.

Pilipović *et al.* [110] identified that polymer parts printed in the x-y plane have improved mechanical strength in comparison to other part layouts. Part fracture during tensile tests for each sample is displayed in Figure 7b. For metallic SL, part strength is lower along the z-axis than along the other direction [108]. Gussev *et al.* [119] showed that mechanical properties such as part strength along the z-axis can be drastically improved by post-printing heat treatments.

Layer thickness also has an influence on the resulting part strength. As explained by Zhang *et al.* [108], mechanical resistance is altered by residual stresses which are influenced by layer thickness.

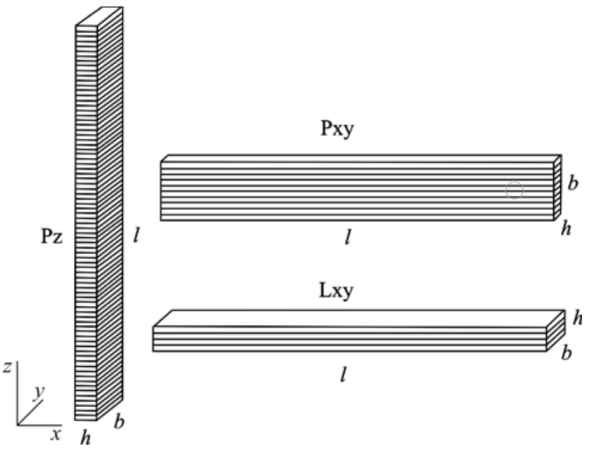

(a)

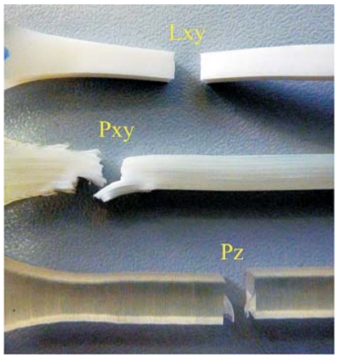

(b)

Fig. 7: SL polymer part layer stacking investigations defined by Pilipović *et al.* [110]: (a) part layer stacking definition; (b) visual comparisons of the sample fracture after tensile tests

Flexural strength

Olivier at al. [120] investigated effect of building orientation in the x-y plane on the flexural strength. Results showed that test parts with a 45° orientation from lamination direction, have higher flexural strength than other layouts.

Fatigue life

Kümmel *et al.* [121] investigated layer deposition and microstructure for composite aluminium sheets in the resulting part fatigue life. Their findings indicated that combining two sheets of aluminium of different mechanical properties resulted in a significant improvement of the part fatigue life.

3.6.4 Summary

Table 8 summarises the SL property review and the influence parameters outlined in the previous section.

3.7 Vat photo-polymerisation

VPP is mainly used in biomedical field [122,123,124] and the process suits for different materials such as polymers [125], ceramics [126] or metals [127].

3.7.1 Geometry and dimensions

As previous AM processes, geometrical and dimensional defects can be declined by dimensional inaccuracy and geometrical deformation.

Dimensional inaccuracy

Williams *et al.* [128] ran several prints with different printing parameters comprising hatching spacing, staircase effect or part width. Authors identified parameters leading to the best part accuracy relative to the nominal geometry definition. In a deeper axis-dependent investigation for polymer samples, Dikova *et al.* [129] outlined a better accuracy in the x-y plane than along the z-axis in comparison to the expected geometry. Moreover, authors also noticed optical properties of photopolymer resin as being of influence in the resulting part geometry. Indeed, due to optical properties such as opacity, photopolymer resins may not be sufficiently cured by polymerising rays. Likewise, polymerising rays maybe reflected, resulting into pronounced curing inaccuracies.

Relying on Taguchi methodology, Zhou *et al.* [130] investigated parameters of influence among layer thickness, layer overcure, hatching space, blade gap and part location on the resulting horizontal and vertical accuracy, geometrical shapes and surface roughness. Authors identified blade gap as having effect on the resulting x or y accuracy. Blade gap refers to the distance between the recoating blade and the last layer being cured. However, authors noticed that the vertical accuracy increases with deeper overcure effects of the scanning laser, i.e. the curing depth reachable by the laser. Geometrical shape accuracy is identified as highly dependent on the chosen layer thickness.

In the same design of experiment, Chockalingam *et al.* [131] considered layer thickness, hatching space and overcure depth on the resulting parallelism, perpendicularity, angularity radius fillet properties. Authors noted parallelism and radius fillet as highly influenced by hatching space whereas perpendicularity was mostly influenced by layer thickness and angularity depended on overcure depth.

Geometrical deformation

VPP parts are subjected to deformation notably by warping and shrinkage effects. Xing *et al.* [132] noticed that warping effect was drastically increased with overall part dimensions. In their works, Li *et al.* [133] highlighted an increased shrinkage along the building direction. That effect is also increased along the length direction. Shrinkage has also been shown to be dependent on the curing hatching space. Indeed, Salmoria *et al.* [134] explained that the high level of hatching space increases volume of uncured resin trapped between layers. This trapped resin results in an increased cure shrinkage effect during post-process steps. Corcione *et al.* [135] showed that shrinkage and curl distortion are increased by lower scan speed. Lower scan speed means that laser polymerises more photopolymer, meaning higher reaction rates.

For ceramic materials, post-process steps are usually water drying, debinding and sintering to reinforce mechanical properties. Zhou *et al.* [136] outlined the use of a desiccant instead of natural drying process to reduce part deformation during that step. Indeed, desiccant allowed a more uniform water removal than natural drying which leads into water evaporation heterogeneity. In the same idea, part shrinkage is mainly due to residual stresses accumulated within the part whilst printing. In order to reduce these residual stresses in ceramic-based parts, Johansson *et al.* [137] showed the advantage of adding non-reactive components in the ceramic suspension.

3.7.2 Surface quality

VPP surface quality works refer to part roughness. Some works compare VPP surface roughness with other AM processes (see [138]). As explained by Cedorge and Colton [139], VPP parts are suited for designing and manufacturing injection moulds. However, increased roughness has an impact on ejection force required as it increases part friction in contact with the mould. That is why, part roughness, which is shown to be dependent on layer thickness, is of major importance for the part application.

Dikova *et al.* [129] measured lower roughness values along the x or y-axis than along the z-axis. Moreover, they assumed photopolymer suspension optical properties to be of influence on the resulting surface roughness. Similar works have been conducted by Xing *et al.* [132].

Some works performed a design of experiment analysis (Taguchi methodology) to identify parameters of influence on the resulting part roughness. Chockalingam *et al.* [131] identified layer thickness as the main parameter impacting the resulting roughness. Zhou *et al.* [130] found the same result. However, they made distinction between lateral surface roughness influenced by layer thickness and top surface roughness influenced not only by layer thickness but also by overcure depth. Khodaii and Rahini [140] measured roughness obtained for different surface tilt angles printed with different hatching spaces. Authors showed the influence of tilt angle and hatching space on roughness values.

Several authors developed part roughness models. Reeves and Cobb [98] established an analytical model to predict roughness values according to the part tilt angle. They could establish a good agreement between their model and measured values from a specific and regularly surface-tilted artefact. Mostafa *et al.* [141] combined staircase predictive models with curing light diffraction models. Results showed that this model is precise to predict surface profile angle, i.e. the angle between previous layer plane and the edge-deposited next layer. However, with a roughness estimation error around 30%, authors outlined the need to improve

the 3D curing model. Singhal *et al.* [142] proposed a roughness predictive model to find the best part orientation within the building volume. Their works identified the best part orientation by minimising the predicted resulting surface roughness. Similarly, Kim and Lee [143] developed a roughness behavioural predictive model. That model estimates resulting part roughness, and minimises post-processing time using a genetic algorithm. It finally provides the user with the optimal advisable layout leading to the lowest post-processing time.

3.7.3 Microstructure

Chugonov *et al.* [144] monitored microstructure evolution in ceramic-based parts during different printing and post-process steps. As described by the authors, green body pores stem either from a lack of homogenisation of the ceramic suspension or air entrapment. With lack of homogenisation, binding material is missing in some area leading to voids after the drying and debinding steps. When removing extra binding material, green body pores grow due to interconnected voids and coalescing effects. During the sintering steps, pores are significantly reduced which increases for example mechanical properties [133]. As described by Johansson *et al.* [137], residual porosity of ceramic-based parts can be reduced by using non-reactive components in the ceramic solution that would not evaporate but decomposed.
Liu *et al.* [145] and Guessasma *et al.* [146] showed the correlation between porosity and mechanical properties as high porosity leads to lower part strength. Moreover, they showed that for designed porosity between 10% and 30%, measured porosity reached lower values than the one expected. This observation is explained as 10% and 30% porosity levels lead to small and closed pores which may trap bonding material. Higher porosity levels result in open porosity where extra bonding material can be easily removed from.

3.7.4 Mechanical properties

Tensile strength
Salmoria *et al.* [147] experienced different post-curing treatments including ultraviolet, microwaves and conventional heating on polymer green parts. Results showed that all these treatments increased mechanical properties. The best improvement is obtained with conventional heating. Authors explained the latter by the uniform stress distribution within the part obtained using conventional heating.

Flexural strength
Additive ceramic-based VPP has been shown to have close flexural strength in comparison with subtractive manufacturing [148]. However, although subtractive and additive parts have close microstructure, porosity is of huge influence on the resulting mechanical properties. Indeed, as shown by Liu *et al.* [145] and Guessasma *et al.* [146], increased porosity decreases the resulting part flexural strength. Moreover, Li *et al.* [133] investigated the effect of sintering temperature for ceramic-based materials on the resulting flexural strength. Based on their works, flexural strength is increased by the increase of sintering temperature. Indeed, as explained by the authors, sintering temperature increase allows the reduction of pore size and then the increase of part homogeneity.

Cracks
Crack formation occurs by the accumulation of residual stresses. As described by Johansson *et al.* [137], they can be minimised by the use of non-reactive components reducing residual stresses. Moreover, Bae and Halloran [149] investigated the effect of residual uncured monomer on end-retract zones on the part cracking behaviour. Indeed, during post-process heating, residual monomer trapped in the end-retract zones may be polymerised resulting in polymerisation shrinkage and cracks. Figure 8 illustrates vertical and horizontal cracks of sintered ceramic part produced by VP and investigated by Bae and Halloran [149].

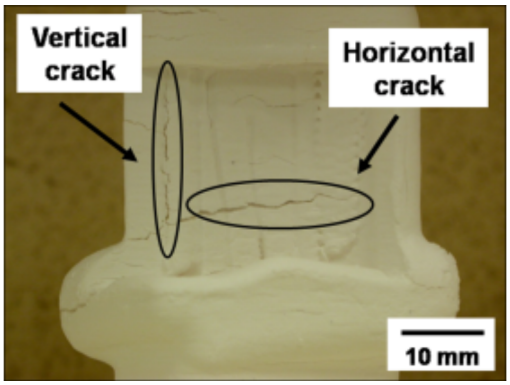

Fig. 8: Illustration of VPP sintered part cracks shown in [149]

3.7.5 Summary

Table 9 summarises the VPP property review, and the influence parameters outlined in the previous section.

4 Discussion

According to this proposed literature review for general AM parts, analysed defect and property families seem to be identical and not depending on the considered AM process. Indeed, AM part defects mainly fall into the fields of geometry and dimensions, microstructure, surface quality or mechanical properties. However, a deeper analysis of these studied properties highlights the declined defects dependency of considered AM process. For example, microstructure studies for DED process mainly focus on grain morphology whereas BJ main works on microstructure relies

	Geometry and dimensions	Surface quality	Microstructure	Mechanical properties
BJ	+++	+	++	+++
DED	++	∅	+++	+++
ME*	+++	+++	++	+++
MJ	+++	+	+	+++
PBF*	+++	+++	+++	+++
SL	+	++	∅	+++
VPP	+++	+++	++	++

* For ME and PBF, estimations of amount of work have been performed according to existing literature reviews (see [85,86,13] for ME, and [10,11,107] for PBF)

Table 2: Summary of amount of works performed for each process category. Amount of work is materialised on a cross typology designed among this literature review. Each evaluation is calculated among the referenced papers relative to the considered AM process: ∅ means that property concerns less than 10% of the referenced papers; + means that property concerns between 10% and 25% of the referenced papers; ++ means that property concerns between 25% and 50% of the referenced papers; +++ means that property concerns more than 50% of the referenced papers

on porosity. In other words, AM defects can always be classified by defect or property family such as geometry and dimensions, microstructure, surface quality or mechanical properties, the latter being commonly defined between AM processes. Nevertheless, declined defects in each of these families for different AM processes can hardly be compared as these AM processes are too different, by the physical property differences involved relative to each AM process.

As revealed in this paper, AM defects and properties have been unequally studied. AM processes were not studied in a generic way but in an adapted-to-the-process way. Table 2 summarises amount of works as reviewed in this paper for all AM process categories. This table provides a quick overview and comparison elements between amount of works for one AM process in comparison with another. Among all seven AM processes, PBF is the most studied process whereas there have been fewer works performed for SL or MJ for example. For approximately all AM process categories, geometry and dimensions, and mechanical properties are the main studied categories. Further works are required in the less studied AM processes, such as SL or MJ microstructure to deeply understand defects and properties of the resulting AM parts and thus provide a more accurate general part defect classification. By taking hindsight, this paper deals with the part-process-material interaction which deep link should be highlighted. AM professions have then evolved into a more communicative requirement and AM design should be anticipated with an interactive objective. This behaviour allows to product optimised and consistent high quality end-use parts in an industrialisation context taking the inherent raised stakes into account [150]. Future works are then required on the production decision making and to develop standard communication roadmaps and process integrations implemented for complex industrial environment, adapted to AM. This roadmap should be based on the process inner and outer complexity in order to increase productibility and by minimising part rejects.

5 Conclusion

This paper proposes a defect and property classification for general AM parts. For general AM parts, common families of defects and properties such as geometry and dimensions, microstructure, surface quality or mechanical properties can be defined. For each family, defects and properties are different according to the each AM process category. Our study gives a better understanding of current research works and proposes a common reference for further comparisons and discussions. This classification is an important mainstay for the designer to rely on and to have a clarified and informed approach of defects affecting a specific process. This classification provides an overview of these defects and allows him to make thoughtful decisions in interaction with the manufacturer regarding the part design. However, as general AM parts are concerned, this encapsulates specific structures such as topology optimised structures or lattice structures. The latter, for instance, consist of a 3D repetition of an elementary pattern. Therefore, it is worth questioning the scale of defects and properties which may impact the classification. Further works will focus on a multi-scale study to identify a relevant and robust classification methodology.

References

1. Gibson, I., Rosen, D. W., and Stucker, B., 2010. *Additive manufacturing technologies: rapid prototyping to direct digital manufacturing*. Springer Verlag.
2. Beyer, C., and Figueroa, D., 2016. "Design and Analysis of Lattice Structures for Additive Manufacturing". *Journal of Manufacturing Science and Engineering,* **138**(12), 09. 121014.
3. Dong, G., Tang, Y., and Zhao, Y. F., 2017. "A Survey of Modeling of Lattice Structures Fabricated by Addi-

tive Manufacturing". *Journal of Mechanical Design,* **139**(10), 08. 100906.
4. Gardan, N., and Schneider, A., 2015. "Topological optimization of internal patterns and support in additive manufacturing". *Journal of Manufacturing Systems,* **37**, pp. 417 – 425.
5. Gao, W., Zhang, Y., Ramanujan, D., Ramani, K., Chen, Y., Williams, C. B., Wang, C. C., Shin, Y. C., Zhang, S., and Zavattieri, P. D., 2015. "The status, challenges, and future of additive manufacturing in engineering". *Computer-Aided Design,* **69**, pp. 65 – 89.
6. Hon, K. K. B., 2007. "Digital additive manufacturing: From rapid prototyping to rapid manufacturing". In Proceedings of the 35th International MATADOR Conference, S. Hinduja and K.-C. Fan, eds., Springer London, pp. 337–340.
7. Ngo, T. D., Kashani, A., Imbalzano, G., Nguyen, K. T., and Hui, D., 2018. "Additive manufacturing (3d printing): A review of materials, methods, applications and challenges". *Composites Part B: Engineering,* **143**, pp. 172 – 196.
8. Bikas, H., Stavropoulos, P., and Chryssolouris, G., 2016. "Additive manufacturing methods and modelling approaches: a critical review". *The International Journal of Advanced Manufacturing Technology,* **83**(1-4), pp. 389–405.
9. Schmidt, M., Merklein, M., Bourell, D., Dimitrov, D., Hausotte, T., Wegener, K., Overmeyer, L., Vollertsen, F., and Levy, G. N., 2017. "Laser based additive manufacturing in industry and academia". *CIRP Annals,* **66**(2), pp. 561 – 583.
10. Malekipour, E., and El-Mounayri, H., 2017. "Common defects and contributing parameters in powder bed fusion am process and their classification for online monitoring and control: a review". *International journal of advanced manufacturing technology,* **95**(1-4), pp. 527–550.
11. Galy, C., Le Guen, E., Lacoste, E., and Arvieu, C., 2018. "Main defects observed in aluminum alloy parts produced by slm: From causes to consequences". *Additive manufacturing,* **22**, pp. 165–175.
12. Snow, Z., Nassar, A., and Reutzel, E., 2020. "Review of the formation and impact of flaws in powder bed fusion additive manufacturing". *Additive Manufacturing,* **36**, 07, p. 101457.
13. Wickramasinghe, S., Do, T., and Tran, P., 2020. "Fdm-based 3d printing of polymer and associated composite: A review on mechanical properties, defects and treatments". *Polymers,* **12**(7), p. 1529.
14. Sanaei, N., and Fatemi, A., 2021. "Defects in additive manufactured metals and their effect on fatigue performance: A state-of-the-art review". *Progress in Materials Science,* **117**, p. 100724.
15. Lakhdar, Y., Tuck, C., Binner, J., Terry, A., and Goodridge, R., 2021. "Additive manufacturing of advanced ceramic materials". *Progress in Materials Science,* **116**, p. 100736.
16. Parandoush, P., and Lin, D., 2017. "A review on additive manufacturing of polymer-fiber composites". *Composite Structures,* **182**, pp. 36–53.
17. Haghdadi, N., Laleh, M., Moyle, M., and Primig, S., 2021. "Additive manufacturing of steels: a review of achievements and challenges". *Journal of Materials Science,* **56**(1), pp. 64–107.
18. Toguem Tagne, S.-C., Rupal, B., Mehdi-Souzani, C., Qureshi, A. J., and Anwer, N., 2018. "A review of am artifact design methods".
19. Li, L., Liu, J., Ma, Y., Ahmad, R., and Qureshi, A., 2019. "Multi-view feature modeling for design-for-additive manufacturing". *Advanced Engineering Informatics,* **39**, pp. 144–156.
20. de Pastre, M.-A., Toguem Tagne, S.-C., and Anwer, N., 2020. "Test artefacts for additive manufacturing: A design methodology review". *CIRP Journal of Manufacturing Science and Technology,* **31**, pp. 14–24.
21. AMT/8, 2016. *BS EN ISO/ASTM 52900:2017 - Additive manufacturing. General principles. Terminology.*
22. Zhang, Y., Wu, L., Guo, X., Kane, S., Deng, Y., Jung, Y.-G., Lee, J.-H., and Zhang, J., 2017. "Additive manufacturing of metallic materials: A review". *Journal of materials engineering and performance,* **27**(1), pp. 1–13.
23. Gokuldoss, P. K., Kolla, S., and Eckert, J., 2017. "Additive manufacturing processes: Selective laser melting, electron beam melting and binder jetting—selection guidelines". *Materials,* **10**(6), p. 672.
24. Ziaee, M., and Crane, N. B., 2019. "Binder jetting: A review of process, materials, and methods". *Additive Manufacturing,* **28**, pp. 781 – 801.
25. Meenashisundaram, G. K., Xu, Z., Nai, M. L. S., Lu, S., Ten, J. S., and Wei, J., 2020. "Binder jetting additive manufacturing of high porosity 316l stainless steel metal foams". *Materials,* **13**(17), p. 3744.
26. Javidani, M., Arreguin-Zavala, J., Danovitch, J., Tian, Y., and Brochu, M., 2016. "Additive manufacturing of alsi10mg alloy using direct energy deposition: Microstructure and hardness characterization". *Journal of thermal spray technology,* **26**(4), pp. 587–597.
27. Turner, B. N., and Gold, S. A., 2015. "A review of melt extrusion additive manufacturing processes: Ii. materials, dimensional accuracy, and surface roughness". *Rapid prototyping journal,* **21**(3), pp. 250–261.
28. Yap, Y. L., Wang, C., Sing, S. L., Dikshit, V., Yeong, W. Y., and Wei, J., 2017. "Material jetting additive manufacturing: An experimental study using designed metrological benchmarks". *Precision Engineering,* **50**, pp. 275 – 285.
29. Zhang, Y., Yang, S., and Zhao, Y. F., 2020. "Manufacturability analysis of metal laser-based powder bed fusion additive manufacturing—a survey". *International journal of advanced manufacturing technology,* **110**(1-2), pp. 57–78.
30. Gong, X., Anderson, T., and Chou, K., 2014. "Review on powder-based electron beam additive manufacturing technology". *Manufacturing review,* **1**, p. 2.
31. Appuhamillage, G. A., Chartrain, N., Meenakshisundaram, V., Feller, K. D., Williams, C. B., and Long, T. E., 2019. "110th anniversary: Vat photopolymerization-based additive manufacturing: Current trends and future directions in materials design". *Industrial & Engineering Chemistry Research,* **58**(33), pp. 15109–15118.
32. Faes, M., Valkenaers, H., Vogeler, F., Vleugels, J., and Ferraris, E., 2015. "Extrusion-based 3d printing of ceramic components". *Procedia Cirp,* **28**, pp. 76–81.
33. Gonzalez-Gutierrez, J., Cano, S., Schuschnigg, S., Kukla, C., Sapkota, J., and Holzer, C., 2018. "Additive manufacturing of metallic and ceramic components by the material extrusion of highly-filled polymers: A review and future perspectives". *Materials,* **11**(5), p. 840.
34. Buswell, R., Leal de Silva, W., Jones, S., and Dirrenberger, J., 2018. "3d printing using concrete extrusion: A roadmap for research". *Cement and Concrete Research,* **112**, pp. 37 – 49. SI : Digital concrete 2018.
35. Thompson, A., 2019. "Surface texture measurement of metal additively manufactured parts by x-ray computed tomography". PhD thesis.
36. Zha, W., and Anand, S., 2015. "Geometric approaches to input file modification for part quality improvement in additive manufacturing". *Journal of Manufacturing Processes,* **20**, pp. 465 – 477. Additive Manufacturing.
37. Bourell, D., Kruth, J. P., Leu, M., Levy, G., Rosen, D., Beese, A. M., and Clare, A., 2017. "Materials for additive manufacturing". *CIRP Annals,* **66**(2), pp. 659 – 681.
38. Król, M., and Tański, T., 2016. "Surface quality research for selective laser melting of ti-6al-4v alloy". *Archives of Metallurgy and Materials,* **61**.

39. Gaytan, S., Cadena, M., Karim, H., Delfin, D., Lin, Y., Espalin, D., MacDonald, E., and Wicker, R., 2015. "Fabrication of barium titanate by binder jetting additive manufacturing technology". *Ceramics International,* **41**(5, Part A), pp. 6610 – 6619.
40. Miyanaji, H., Momenzadeh, N., and Yang, L., 2019. "Effect of powder characteristics on parts fabricated via binder jetting process". *Rapid prototyping journal,* **25**(2), pp. 332–342.
41. Lores, A., Azurmendi, N., Agote, I., and Zuza, E., 2019. "A review on recent developments in binder jetting metal additive manufacturing: materials and process characteristics". *Powder metallurgy,* **62**(5), pp. 267–296.
42. Cao, S., Qiu, Y., Wei, X.-F., and Zhang, H.-H., 2015. "Experimental and theoretical investigation on ultra-thin powder layering in three dimensional printing (3dp) by a novel double-smoothing mechanism". *Journal of materials processing technology,* **220**, pp. 231–242.
43. Hsu, T., and Lai, W., 2010. "Manufacturing parts optimization in the three-dimensional printing process by the taguchi method". *Journal of the Chinese Institute of Engineers,* **33**(1), pp. 121–130.
44. Miyanaji, H., Momenzadeh, N., and Yang, L., 2018. "Effect of printing speed on quality of printed parts in binder jetting process". *Additive Manufacturing,* **20**, pp. 1 – 10.
45. Miyanaji, H., Zhang, S., Lassell, A., Zandinejad, A. A., and Yang, L., 2016. "Optimal process parameters for 3d printing of porcelain structures". *Procedia Manufacturing,* **5**, pp. 870 – 887. 44th North American Manufacturing Research Conference, NAMRC 44, June 27-July 1, 2016, Blacksburg, Virginia, United States.
46. Chavez, L. A., Ibave, P., Wilburn, B., Alexander, D., Stewart, C., Wicker, R., and Lin, Y., 2020. "The influence of printing parameters, post-processing, and testing conditions on the properties of binder jetting additive manufactured functional ceramics". *Ceramics,* **3**(1), pp. 65–77.
47. Chen, H., and Zhao, Y. F., 2016. "Process parameters optimization for improving surface quality and manufacturing accuracy of binder jetting additive manufacturing process". *Rapid prototyping journal,* **22**(3), pp. 527–538.
48. Wang, Y., and Zhao, Y. F., 2017. "Investigation of sintering shrinkage in binder jetting additive manufacturing process". *Procedia Manufacturing,* **10**, pp. 779 – 790. 45th SME North American Manufacturing Research Conference, NAMRC 45, LA, USA.
49. , 2000. *BS EN ISO 4287:1998+A1:2009: Geometrical product specification (GPS). Surface texture: Profile method. Terms, definitions and surface texture parameters.* British Standards Institute.
50. Do, T., Shin, C. S., Stetsko, D., VanConant, G., Vartanian, A., Pei, S., and Kwon, P., 2015. "Improving structural integrity with boron-based additives for 3d printed 420 stainless steel". *Procedia manufacturing,* **1**, pp. 263–272.
51. Asadi-Eydivand, M., Solati-Hashjin, M., Farzad, A., and Abu Osman, N. A., 2016. "Effect of technical parameters on porous structure and strength of 3d printed calcium sulfate prototypes". *Robotics and Computer-Integrated Manufacturing,* **37**, pp. 57 – 67.
52. Mostafaei, A., Toman, J., Stevens, E. L., Hughes, E. T., Krimer, Y. L., and Chmielus, M., 2017. "Microstructural evolution and mechanical properties of differently heat-treated binder jet printed samples from gas- and water-atomized alloy 625 powders". *Acta materialia,* **124**, pp. 280–289.
53. Zhu, Y., Wu, Z., Hartley, W. D., Sietins, J. M., Williams, C. B., and Yu, H. Z., 2020. "Unraveling pore evolution in post-processing of binder jetting materials: X-ray computed tomography, computer vision, and machine learning". *Additive manufacturing,* **34**, p. 101183.
54. Chumnanklang, R., Panyathanmaporn, T., Sitthiseripratip, K., and Suwanprateeb, J., 2007. "3d printing of hydroxyapatite: Effect of binder concentration in pre-coated particle on part strength". *Materials Science and Engineering: C,* **27**(4), pp. 914 – 921.
55. Doyle, M., Agarwal, K., Sealy, W., and Schull, K., 2015. "Effect of layer thickness and orientation on mechanical behavior of binder jet stainless steel 420 + bronze parts". *Procedia Manufacturing,* **1**, pp. 251 – 262. 43rd North American Manufacturing Research Conference, NAMRC 43, 8-12 June 2015, UNC Charlotte, North Carolina, United States.
56. Chabot, A., Laroche, N., Carcreff, E., Rauch, M., and Hascoët, J.-Y., 2019. "Towards defect monitoring for metallic additive manufacturing components using phased array ultrasonic testing". *Journal of Intelligent Manufacturing*, pp. 1–11.
57. Everton, S. K., Hirsch, M., Stravroulakis, P., Leach, R. K., and Clare, A. T., 2016. "Review of in-situ process monitoring and in-situ metrology for metal additive manufacturing". *Materials and Design,* **95**, pp. 431 – 445.
58. Kim, H., Lin, Y., and Tseng, T.-L. B., 2018. "A review on quality control in additive manufacturing". *Rapid prototyping journal,* **24**(3), pp. 645–669.
59. Bi, G., Gasser, A., Wissenbach, K., Drenker, A., and Poprawe, R., 2006. "Characterization of the process control for the direct laser metallic powder deposition". *Surface & coatings technology,* **201**(6), pp. 2676–2683.
60. Masaylo, D., Igoshin, S., Popovich, A., and Popovich, V., 2020. "Effect of process parameters on defects in large scale components manufactured by direct laser deposition". *Materials today : proceedings,* **30**, pp. 665–671.
61. Atwood, C., Griffith, M., Harwell, L., Schlienger, E., Ensz, M., Smugeresky, J., Romero, T., Greene, D., and Reckaway, D., 1998. "Laser engineered net shaping (lens™): A tool for direct fabrication of metal parts". In International Congress on Applications of Lasers & Electro-Optics, Vol. 1998, Laser Institute of America, pp. E1–E7.
62. Heralić, A., Christiansson, A.-K., and Lennartson, B., 2012. "Height control of laser metal-wire deposition based on iterative learning control and 3d scanning". *Optics and lasers in engineering,* **50**(9), pp. 1230–1241.
63. Chabot, A., 2020. "Methodology for multi-physical monitoring of ded processes: development via an experimental approach". PhD thesis.
64. Toyserkani, E., and Khajepour, A., 2006. "A mechatronics approach to laser powder deposition process". *Mechatronics (Oxford),* **16**(10), pp. 631–641.
65. Shamsaei, N., Yadollahi, A., Bian, L., and Thompson, S. M., 2015. "An overview of direct laser deposition for additive manufacturing; part ii: Mechanical behavior, process parameter optimization and control". *Additive Manufacturing,* **8**, pp. 12–35.
66. Razavi, S. M. J., and Berto, F., 2019. "Directed energy deposition versus wrought ti-6al-4v: A comparison of microstructure, fatigue behavior, and notch sensitivity". *Advanced engineering materials,* **21**(8), pp. 1900220–n/a.
67. Saboori, A., Gallo, D., Biamino, S., Fino, P., and Lombardi, M., 2017. "An overview of additive manufacturing of titanium components by directed energy deposition: Microstructure and mechanical properties". *Applied sciences,* **7**(9), p. 883.
68. Zhu, Y., Liu, D., Tian, X., Tang, H., and Wang, H., 2014. "Characterization of microstructure and mechanical properties of laser melting deposited ti–6.5al–3.5mo–1.5zr–0.3si titanium alloy". *Materials in engineering,* **56**, pp. 445–453.
69. Chen, B., Huang, Y., Gu, T., Tan, C., and Feng, J., 2018. "Investigation on the process and microstructure evolution during direct laser metal deposition of

18ni300". *Rapid prototyping journal,* **24**(6), pp. 964–972.
70. Manjaiah, M., Hascoët, J., and Rauch, M., 2020. "Effect of process parameters on track geometry, microstructural evolution on 316l stainless steel multi-layer clads". *Materials Science and Engineering: B,* **259**, p. 114583.
71. El Cheikh, H., Courant, B., Branchu, S., Huang, X., Hascoët, J.-Y., and Guillén, R., 2012. "Direct laser fabrication process with coaxial powder projection of 316l steel. geometrical characteristics and microstructure characterization of wall structures". *Optics and Lasers in Engineering,* **50**(12), pp. 1779–1784.
72. Zhang, X., Li, W., Chen, X., Cui, W., and Liou, F., 2017. "Evaluation of component repair using direct metal deposition from scanned data". *International journal of advanced manufacturing technology,* **95**(9-12), pp. 3335–3348.
73. Selcuk, C., 2011. "Laser metal deposition for powder metallurgy parts". *Powder metallurgy,* **54**(2), pp. 94–99.
74. Liu, C., Tian, X., Tang, H., and Wang, H., 2013. "Microstructural characterization of laser melting deposited ti–5al-5mo–5v–1cr–1fe near β titanium alloy". *Journal of alloys and compounds,* **572**, pp. 17–24.
75. Zhang, P., Zhou, X., Cheng, X., Sun, H., Ma, H., and Li, Y., 2020. "Elucidation of bubble evolution and defect formation in directed energy deposition based on direct observation". *Additive manufacturing,* **32**, p. 101026.
76. Gaja, H., Gaja, H., Liou, F., and Liou, F., 2017. "Defects monitoring of laser metal deposition using acoustic emission sensor". *International journal of advanced manufacturing technology,* **90**(1), pp. 561–574.
77. Rauch, M., Hascoët, J.-Y., and Mallaiah, M., 2020. "Repairing ti-6al-4v aeronautical components with ded additive manufacturing". In MATEC Web of Conferences, Vol. 321, EDP Sciences, p. 03017.
78. Chabot, A., Laroche, N., Carcreff, E., Rauch, M., and Hascoët, J.-Y., 2019. "Towards defect monitoring for metallic additive manufacturing components using phased array ultrasonic testing". *Journal of intelligent manufacturing,* **31**(5), pp. 1191–1201.
79. Klein, M., and Sears, J., 2004. "Laser ultrasonic inspection of laser cladded 316lss and ti-6-4". In International Congress on Applications of Lasers & Electro-Optics, Vol. 2004, Laser Institute of America, p. 1006.
80. Wang, F., Mao, H., Zhang, D., Zhao, X., and Shen, Y., 2008. "Online study of cracks during laser cladding process based on acoustic emission technique and finite element analysis". *Applied surface science,* **255**(5), pp. 3267–3275.
81. Rangaswamy, P., Griffith, M., Prime, M., Holden, T., Rogge, R., Edwards, J., and Sebring, R., 2005. "Residual stresses in lens ® components using neutron diffraction and contour method". pp. 72–83.
82. Dai, K., and Shaw, L., 2002. "Distortion minimization of laser-processed components through control of laser scanning patterns". *Rapid prototyping journal,* **8**(5), pp. 270–276.
83. Bandyopadhyay, A., Upadhyayula, M., Traxel, K. D., and Onuike, B., 2019. "Influence of deposition orientation on fatigue response of lens™ processed ti6al4v". *Materials Letters,* **255**, p. 126541.
84. Penumakala, P. K., Santo, J., and Thomas, A., 2020. "A critical review on the fused deposition modeling of thermoplastic polymer composites". *Composites Part B: Engineering,* **201**, p. 108336.
85. Agarwala, M. K., Jamalabad, V. R., Langrana, N. A., Safari, A., Whalen, P. J., and Danforth, S. C., 1996. "Structural quality of parts processed by fused deposition". *Rapid prototyping journal,* **2**(4), pp. 4–19.
86. Papazetis, G., and Vosniakos, G.-C., 2018. "Mapping of deposition-stable and defect-free additive manufacturing via material extrusion from minimal experiments". *International journal of advanced manufacturing technology,* **100**(9-12), pp. 2207–2219.
87. Tay, Y. W. D., Panda, B., Paul, S., Noor Mohamed, N. A., Tan, M., and Leong, K. F., 2017. "3d printing trends in building and construction industry: a review". *Virtual and Physical Prototyping*, 04.
88. Paul, S., van Zijl, G., Tan, M., and Gibson, I., 2018. "A review of 3d concrete printing systems and materials properties: current status and future research prospects". *Rapid Prototyping Journal,* **24**, 04, pp. 00–00.
89. Vaezi, M., Chianrabutra, S., Mellor, B., and Yang, S., 2013. "Multiple material additive manufacturing – part 1: A review". *Virtual and Physical Prototyping,* **8**, 03.
90. Tourloukis, G., Stoyanov, S., Tilford, T., and Bailey, C., 2015. "Data driven approach to quality assessment of 3d printed electronic products". In 2015 38th International Spring Seminar on Electronics Technology (ISSE), IEEE, pp. 300–305.
91. Sturm, L. D., Albakri, M. I., Tarazaga, P. A., and Williams, C. B., 2019. "In situ monitoring of material jetting additive manufacturing process via impedance based measurements". *Additive manufacturing,* **28**, pp. 456–463.
92. Ebert, J., Özkol, E., Zeichner, A., Uibel, K., Weiss, O., Koops, U., Telle, R., and Fischer, H., 2009. "Direct inkjet printing of dental prostheses made of zirconia". *Journal of dental research,* **88**(7), pp. 673–676.
93. Khoshkhoo, A., Carrano, A. L., and Blersch, D. M., 2018. "Effect of build orientation and part thickness on dimensional distortion in material jetting processes". *Rapid prototyping journal,* **24**(9), pp. 1563–1571.
94. Cazón, A., Morer, P., and Matey, L., 2014. "Polyjet technology for product prototyping: Tensile strength and surface roughness properties". *Proceedings of the Institution of Mechanical Engineers. Part B, Journal of engineering manufacture,* **228**(12), pp. 1664–1675.
95. Pugalendhi, A., Ranganathan, R., and Chandrasekaran, M., 2020. "Effect of process parameters on mechanical properties of veroblue material and their optimal selection in polyjet technology". *International journal of advanced manufacturing technology,* **108**(4), pp. 1049–1059.
96. Kechagias, J. D., and Maropoulos, S., 2015. "An investigation of sloped surface roughness of direct poly-jet 3d printing". In Proceedings of the International Conference on Industrial Engineering—INDE, pp. 150–153.
97. Kumar, K., and Kumar, G. S., 2015. "An experimental and theoretical investigation of surface roughness of poly-jet printed parts". *Virtual and Physical Prototyping,* **10**(1), pp. 23–34.
98. Reeves, P. E., and Cobb, R. C., 1997. "Reducing the surface deviation of stereolithography using in-process techniques". *Rapid prototyping journal,* **3**(1), pp. 20–31.
99. Strano, G., Hao, L., Everson, R. M., and Evans, K. E., 2013. "Surface roughness analysis, modelling and prediction in selective laser melting". *Journal of Materials Processing Technology,* **213**(4), pp. 589 – 597.
100. Townsend, A., Senin, N., Blunt, L., Leach, R., and Taylor, J., 2016. "Surface texture metrology for metal additive manufacturing: a review". *Precision Engineering,* **46**, pp. 34 – 47.
101. Udroiu, R., Braga, I., and Nedelcu, A., 2019. "Evaluating the quality surface performance of additive manufacturing systems: Methodology and a material jetting case study". *Materials,* **12**(6), p. 995.
102. Chen, Y., and Lu, J., 2012. "Rp part surface quality versus build orientation: When the layers are getting thinner". *The International Journal of Advanced Manufacturing Technology,* **67**, 07.
103. Moore, J. P., and Williams, C. B., 2015. "Fatigue properties of parts printed by polyjet material jetting". *Rapid prototyping journal,* **21**(6), pp. 675–685.
104. Bass, L., Meisel, N. A., and Williams, C. B., 2016. "Exploring variability of orientation and aging effects in ma-

terial properties of multi-material jetting parts". *Rapid prototyping journal,* **22**(5), pp. 826–834.
105. Vu, I. Q., Bass, L. B., Williams, C. B., and Dillard, D. A., 2018. "Characterizing the effect of print orientation on interface integrity of multi-material jetting additive manufacturing". *Additive manufacturing,* **22**, pp. 447–461.
106. Kaweesa, D. V., and Meisel, N. A., 2018. "Quantifying fatigue property changes in material jetted parts due to functionally graded material interface design". *Additive manufacturing,* **21**, pp. 141–149.
107. Vo, T., Museau, M., Vignat, F., Villeneuve, F., Ledoux, Y., and Ballu, A., 2018. "Typology of geometrical defects in electron beam melting". *Procedia CIRP,* **75**, pp. 92–97.
108. Zhang, Y., Wu, L., Guo, X., Kane, S., Deng, Y., Jung, Y.-G., Lee, J.-H., and Zhang, J., 2017. "Additive manufacturing of metallic materials: A review". *Journal of materials engineering and performance,* **27**(1), pp. 1–13.
109. Dermeik, B., and Travitzky, N., 2020. "Laminated object manufacturing of ceramic-based materials". *Advanced engineering materials,* **22**(9), pp. 2000256–n/a.
110. Pilipović, A., Raos, P., and Šercer, M., 2011. "Experimental testing of quality of polymer parts produced by laminated object manufacturing–lom". *Tehnički vjesnik,* **18**(2), pp. 253–260.
111. Kechagias, J., 2007. "An experimental investigation of the surface roughness of parts produced by lom process". *Rapid Prototyping Journal,* **13**, 01, pp. 17–22.
112. Bhatt, P. M., Kabir, A. M., Peralta, M., Bruck, H. A., and Gupta, S. K., 2019. "A robotic cell for performing sheet lamination-based additive manufacturing". *Additive Manufacturing,* **27**, pp. 278 – 289.
113. Kechagias, J., 2007. "Investigation of lom process quality using design of experiments approach". *Rapid prototyping journal,* **13**(5), pp. 316–323.
114. Chryssolouris, G., Kechagias, J. D., Kotselis, J. L., Mourtzis, D. A., and Zannis, S. G., 1999. "Surface roughness modelling of the helisys laminated object manufacturing (lom) process". In 8th European Conference on Rapid Prototyping and Manufacturing, Nottingham, pp. 141–152.
115. Paul, B. K., and Voorakarnam, V., 2001. "Effect of layer thickness and orientation angle on surface roughness in laminated object manufacturing". *Journal of manufacturing processes,* **3**(2), pp. 94–101.
116. Ahn, D., Kweon, J.-H., Choi, J., and Lee, S., 2012. "Quantification of surface roughness of parts processed by laminated object manufacturing". *Journal of Materials Processing Technology,* **212**(2), pp. 339–346.
117. Chryssolouris, G., Kechagias, J., Moustakas, P., and Koutras, E., 2003. "An experimental investigation of the tensile strength of parts produced by laminated object manufacturing (lom) process". Vol. 32.
118. Zhang, Y., and Wang, J., 2017. "Fabrication of functionally graded porous polymer structures using thermal bonding lamination techniques". *Procedia manufacturing,* **10**, pp. 866–875.
119. Gussev, M., Sridharan, N., Norfolk, M., Terrani, K., and Babu, S., 2017. "Effect of post weld heat treatment on the 6061 aluminum alloy produced by ultrasonic additive manufacturing". *Materials science & engineering. A, Structural materials : properties, microstructure and processing,* **684**(C), pp. 606–616.
120. Olivier, D., Travieso-Rodriguez, J. A., Borros, S., Reyes, G., and Jerez-Mesa, R., 2017. "Influence of building orientation on the flexural strength of laminated object manufacturing specimens". *Journal of mechanical science and technology,* **31**(1), pp. 133–139.
121. Kummel, F., Hausöl, T., Höppel, H. W., and Göken, M., 2016. "Enhanced fatigue lives in aa1050a/aa5005 laminated metal composites produced by accumulative roll bonding". *Acta materialia,* **120**, pp. 150–158.
122. Melchels, F. P., Feijen, J., and Grijpma, D. W., 2010. "A review on stereolithography and its applications in biomedical engineering". *Biomaterials,* **31**(24), pp. 6121–6130.
123. Chen, P., Zheng, L., Wang, Y., Tao, M., Xie, Z., Xia, C., Gu, C., Chen, J., Qiu, P., Mei, S., Ning, L., Shi, Y., Fang, C., Fan, S., and Lin, X., 2019. "Desktop-stereolithography 3d printing of a radially oriented extracellular matrix/mesenchymal stem cell exosome bioink for osteochondral defect regeneration". *Theranostics,* **9**(9), pp. 2439–2459.
124. Luo, Y., Pan, H., Jiang, J., Zhao, C., Zhang, J., Chen, P., Lin, X., and Fan, S., 2020. "Desktop-stereolithography 3d printing of a polyporous extracellular matrix bioink for bone defect regeneration". *Frontiers in Bioengineering and Biotechnology,* **8**, p. 1300.
125. Tan, L. J., Zhu, W., and Zhou, K., 2020. "Recent progress on polymer materials for additive manufacturing". *Advanced Functional Materials,* **30**(43), p. 2003062.
126. Lee, J. W., Lee, I. H., and Cho, D.-W., 2006. "Development of micro-stereolithography technology using metal powder". *Microelectronic engineering,* **83**(4-9), pp. 1253–1256.
127. Halloran, J. W., 2016. "Ceramic stereolithography: Additive manufacturing for ceramics by photopolymerization". *Annual review of materials research,* **46**(1), pp. 19–40.
128. Williams, R., Komaragiri, S., Melton, V., and Bishu, R., 1996. "Investigation of the effect of various build methods on the performance of rapid prototyping (stereolithography)". *Journal of materials processing technology,* **61**(1-2), pp. 173–178.
129. Dikova, T., Dzhendov, D., Katreva, I., Pavlova, D., Tonchev, T., and Doychinova, M., 2017. "Geometry and surface roughness of polymeric samples produced by stereolithography". *Int J Mach Tech Mat,* **4**, pp. 201–5.
130. Zhou, J. G., Herscovici, D., and Chen, C. C., 2000. "Parametric process optimization to improve the accuracy of rapid prototyped stereolithography parts". *International Journal of Machine Tools and Manufacture,* **40**(3), pp. 363–379.
131. Chockalingam, K., Jawahar, N., Chandrasekhar, U., Praveen, J., and Karthic, M., 2016. "Development of process model for optimal selection of process parameters for geometric tolerances and surface roughness in stereolithography.". *International Journal of Advanced Design & Manufacturing Technology,* **9**(3).
132. Xing, H., Zou, B., Li, S., and Fu, X., 2017. "Study on surface quality, precision and mechanical properties of 3d printed zro2 ceramic components by laser scanning stereolithography". *Ceramics International,* **43**(18), pp. 16340–16347.
133. Li, H., Liu, Y., Liu, Y., Hu, K., Lu, Z., and Liang, J., 2020. "Influence of sintering temperature on microstructure and mechanical properties of al_2o3 ceramic via 3d stereolithography". *Acta Metallurgica Sinica (English Letters),* **33**(2), pp. 204–214.
134. Salmoria, G., Ahrens, C., Beal, V., Pires, A., and Soldi, V., 2009. "Evaluation of post-curing and laser manufacturing parameters on the properties of somos 7110 photosensitive resin used in stereolithography". *Materials & Design,* **30**(3), pp. 758 – 763.
135. Corcione, C. E., Greco, A., and Maffezzoli, A., 2006. "Temperature evolution during stereolithography building with a commercial epoxy resin". *Polymer Engineering & Science,* **46**(4), pp. 493–502.
136. Zhou, M., Liu, W., Wu, H., Song, X., Chen, Y., Cheng, L., He, F., Chen, S., and Wu, S., 2016. "Preparation of a defect-free alumina cutting tool via additive manufacturing based on stereolithography – optimization of the drying and debinding processes". *Ceramics International,* **42**(10), pp. 11598 – 11602.

137. Johansson, E., Lidström, O., Johansson, J., Lyckfeldt, O., and Adolfsson, E., 2017. "Influence of resin composition on the defect formation in alumina manufactured by stereolithography". *Materials,* **10**(2), p. 138.
138. Dikova, T., Dzhendov, D., Ivanov, D., and Bliznakova, K., 2018. "Dimensional accuracy and surface roughness of polymeric dental bridges produced by different 3d printing processes". *Arch Mater Sci Eng,* **94**, pp. 65–75.
139. Cedorge, T., and Colton, J., 2000. "Draft angle and surface roughness effects on stereolithography molds". *Polymer Engineering & Science,* **40**(7), pp. 1581–1588.
140. Khodaii, J., and Rahimi, A. "Improving the surface roughness in stereolithography by controlling surface angle, hatch spaces, and postcuring time". *Engineering Reports*, p. e12193.
141. Mostafa, K. G., Nobes, D. S., and Qureshi, A. J., 2020. "Investigation of light-induced surface roughness in projection micro-stereolithography additive manufacturing (pμsla)". *Procedia CIRP,* **92**, pp. 187–193.
142. Singhal, S., Pandey, A., Pandey, P., and Nagpal, A., 2005. "Optimum part deposition orientation in stereolithography". *Computer-Aided Design and Applications,* **2**(1-4), pp. 319–328.
143. Kim, H.-C., and Lee, S.-H., 2005. "Reduction of post-processing for stereolithography systems by fabrication-direction optimization". *Computer-Aided Design,* **37**(7), pp. 711–725.
144. Chugunov, S., Adams, N. A., and Akhatov, I., 2020. "Evolution of sla-based al2o3 microstructure during additive manufacturing process". *Materials,* **13**(18), p. 3928.
145. Liu, T., Guessasma, S., Zhu, J., Zhang, W., Nouri, H., and Belhabib, S., 2018. "Microstructural defects induced by stereolithography and related compressive behaviour of polymers". *Journal of Materials Processing Technology,* **251**, pp. 37–46.
146. Guessasma, S., Tao, L., Belhabib, S., Zhu, J., Zhang, W., and Nouri, H., 2018. "Analysis of microstructure and mechanical performance of polymeric cellular structures designed using stereolithography". *European Polymer Journal,* **98**, pp. 72–82.
147. Salmoria, G., Ahrens, C., Fredel, M., Soldi, V., and Pires, A., 2005. "Stereolithography somos 7110 resin: mechanical behavior and fractography of parts post-cured by different methods". *Polymer Testing,* **24**(2), pp. 157 – 162.
148. Lu, Y., Mei, Z., Zhang, J., Gao, S., Yang, X., Dong, B., Yue, L., and Yu, H., 2020. "Flexural strength and weibull analysis of y-tzp fabricated by stereolithographic additive manufacturing and subtractive manufacturing". *Journal of the European Ceramic Society,* **40**(3), pp. 826 – 834.
149. Bae, C.-J., and Halloran, J. W., 2011. "Influence of residual monomer on cracking in ceramics fabricated by stereolithography". *International journal of applied ceramic technology,* **8**(6), pp. 1289–1295.
150. Dilberoglu, U. M., Gharehpapagh, B., Yaman, U., and Dolen, M., 2017. "The role of additive manufacturing in the era of industry 4.0". *Procedia Manufacturing,* **11**, pp. 545–554. 27th International Conference on Flexible Automation and Intelligent Manufacturing, FAIM2017, 27-30 June 2017, Modena, Italy.

Tables

Properties and defects		Influenced by
Geometry and dimensions	Dimensional inaccuracy	Layer spread (Lores *et al.* [41]; Cao *et al.* [42]) Part localisation (Hsu *et al.* [43]) Printing speed (Miyanaji *et al.* [44]) Drying power (Miyanaji *et al.* [45]) Final grain size (Chavez *et al.* [46])
	Geometrical deformation	Drying time (Chen and Zaho [47]) Considered axis (Wang and Zaho [48]) Sintering conditions (Wang and Zaho [48])
Surface quality	Surface roughness	Layer thickness (Chen and Zaho [47]) Binder saturation (Lores *et al.* [41]; Chen and Zaho [47]) Particle size (Miyanaji *et al.* [40]) Sintering (Do *et al.* [50])
Microstructure	Porosity	Part orientation (Asadi-Eydivand *et al.* [51]) Layer thickness (Asadi-Eydivand *et al.* [51]) Delay time (Asadi-Eydivand *et al.* [51]) Particle shape (Mostafaei *et al.* [52]) Densification (Zhu *et al.* [53]) Sintering temperature (Chavez *et al.* [46]; Do *et al.* [50])
Mechanical	Strength	Particle size (Miyanaji *et al.* [40]; Chumnanklang *et al.* [54]) Binder saturation (Miyanaji *et al.* [40]; Hsu *et al.* [43]; Chavez *et al.* [46]; Chumnanklang *et al.* [54]) Printing speed (Miyanaji *et al.* [44]) Layer thickness (Doyle *et al.* [55]) Density (Doyle *et al.* [55]) Sintering (Chumnanklang *et al.* [54])
	Cracks	First layer shear efforts (Lores *et al.* [41]) Powder distribution strategy (Lores *et al.* [41]) Drying power (Lores *et al.* [41])
Electrical	-	Sintering temperature (Chavez *et al.* [46]) Part orientation (Chavez *et al.* [46])

Table 3: Proposed BJ property and defect classification according to main BJ works

Properties and defects		Influenced by
Geometry and dimensions	Dimensional inaccuracy	Size and temperature of melt pool (Bi *et al.* [59]) Low deposition rate (Masaylo *et al.* [60]) Layer thickness (Atwood *et al.* [61])
	Geometrical deformation	Cooling rate (Bi *et al.* [59])
Surface quality	Roughness	-
Microstructure	Morphology	Temperature gradients and solidification rates (Shamsaei *et al.* [65]; Saboori *et al.* [67]; Selcuk [73]) Layer stacking (Saboori *et al.* [67]; Liu *et al.* [74]) Discontinuity (Zhang *et al.* [72])
	Oxide inclusion	Trapped gas (Masaylo *et al.* [60])
	Porosity	Trapped gas and bubble release (Zhang *et al.* [75]) Interlayer porosity (Everton *et al.* [57]; Masaylo *et al.* [60])
Mechanical	Strength	Printing orientations (Shamsaei *et al.* [65]; Saboori *et al.* [67]) Cooling rates (Shamsaei *et al.* [65]; Saboori *et al.* [67])
	Cracks	Material thickness (Wang *et al.* [80]) Cooling rates (Wang *et al.* [80])
	Hardness	Microstructure (Javidani *et al.* [26]; Zhang *et al.* [72])
	Residual stresses	Laser direction (Rangaswamy *et al.* [81]) Position in the sample (centre/edge) (Shamsaei *et al.* [65]; Rangaswamy *et al.* [81]) Distance-to-substrate (Shamsaei *et al.* [65]) Thermal gradients (Shamsaei *et al.* [65]) Scan strategy (Rangaswamy *et al.* [81])
	Fatigue life	Grain size (Razavi *et al.* [66])

Table 4: Proposed DED property and defect classification according to main DED works

Properties and defects		Influenced by
Geometry and dimensions	Dimensional inaccuracy	Start/stop errors (Agarwala *et al.* [85]) Chordal errors (Agarwala *et al.* [85]) Support structure removal (Agarwala *et al.* [85])
	Geometrical deformations	Deformed edges (Papazatis and Vosniakos [86]) Base bulging (Papazatis and Vosniakos [86]) Thermal gradient (Wickramasinghe *et al.* [13])
Surface quality	Roughness	Staircase effect (Agarwala *et al.* [85]; Wickramasinghe *et al.* [13]) Top/bottom surfaces (Agarwala *et al.* [85]) Start/stop errors (Agarwala *et al.* [85]) Support structure removal (Agarwala *et al.* [85])
Microstructure	Voids	Sharp turns (Agarwala *et al.* [85]) Path strategy (Agarwala *et al.* [85]) Fibre insertion strategy (Wickramasinghe *et al.* [13])
Mechanical	Strength	Weak interface (Agarwala *et al.* [85]; Papazetis and Vosniakos [86]; Wickramasinghe *et al.* [13]) Filament diameter variation (Agarwala *et al.* [85])-Flow tweak (Papazetis and Vosniakos [86]) Underflow and filament slippage (Agarwala *et al.* [85])
	Cracks	Weak interface (Agarwala *et al.* [85])

Table 5: Classification of reviewed ME defects

Properties and defects		Influenced by
Geometry and dimensions	Dimensional inaccuracy	Shape of droplets (Vaezi *et al.* [89]) Droplet ejection,deposition and solidification (Tourloukis *et al.* [90])
	Geometrical deformation	Part thickness and orientation (Koshkhoo *et al.* [93]) Residual stresses (Koshkhoo *et al.* [93])
Surface quality	Roughness	Part tilt angle (Keshagias and Maropoulos [96], Udroiu *et al.* [101]) Surface finish (Cazon *et al.* [94], Kumar and Saravana Kumar [97], Udroiu *et al.* [101])
Microstructure	Voids	(Moore and Williams [103])
Mechanical	Strength	Part orientation (Cazón *et al.* [94]; Bass *et al.* [104]; Vu *et al.* [105])
	Fatigue	Quality and surface finish (Pugalendhi *et al.* [95]) Surface finish (Moore and Williams [103]) Multimaterial gradient type and length (Kaweesa and Meisel [106])
	Ageing	Time (Bass *et al.* [104])

Table 6: Proposed MJ property and defect classification according to main MJ works

Properties and defects		Influenced by
Geometry and dimensions	Form	Staircase Machine errors
	Size	Tap density Shrinkage Spot diameter Microstructural waviness Building direction Gas flow rate
Surface quality	Surface roughness	Scan strategy/laser specifications Powder deposition Pits on the surface Fractures, cracks and holes Quality of substrate Staircase effects Surface orientation
	Balling	Energy density Used gas Cooling rate Powder effect Plateau's coefficient Poor wetting
	Surface deformation	Warping Layer distortion
	Surface oxidation	-
Microstructure	Anisotropy	Scan direction Layer orientation
	Heterogeneity	Powder conditioning Scan strategy Energy density Temperature Solidification condition
	Porosity	Laser specification Laser mode(pulsed...) Scan strategy Balling Powder morphology Drying treatment Layer thickness Melt pool size Poor wetting Powder packing density Overlapping ratio Entrapped gas Layer orientation Densification Gas flow conditions
Mechanical	-	Fracture/cracks/holes Inter-layer bonding Porosity Low strength Stiffness Residual stresses

Table 7: LPBF defect classification proposed by Malekipour and El-Mounayri [10]

Properties and defects		Influenced by
Geometry and dimensions	Dimensional inaccuracy	Heater rolling speed (Kechagias [113]) Part position towards lamination direction (Pilipović *et al.* [110]) Sonotrode bonding effect (for metal sheets-Zhang *et al.* [108])
Surface quality	Roughness	Part position towards lamination direction (Pilipović *et al.* [110]) Heated roller temperature (Kechagias [111]) Tilt angle and layer thickness (Chryssolouris *et al.* [114]; Paul and Voorakarnam [115]; Ahn *et al.* [116]) Penetration depth (Ahn *et al.* [116])
Microstructure	-	-
Mechanical	Tensile Strength	Layer thickness (Chryssolouris *et al.* [117]) Bonding strength and compression time (Zhang and Wang [118]) Part position towards lamination direction (Pilipović *et al.* [110]) Laminated part direction (Zhang *et al.* [108]) Heat treatment (Gussev *et al.* [119])
	Flexural strength	Part orientation in x-y plane (Olivier *et al.* [120])
	Fatigue	Composite lamination (Kümmel *et al.* [121])

Table 8: Proposed SL property and defect classification according to main SL works

Properties and defects		Influenced by
Geometry and dimensions	Dimensional inaccuracy	Considered axis (Dikova *et al.* [129]; Zhou *et al.* [130])) Blade gap (Zhou *et al.* [130]) Layer thickness (Zhou *et al.* [130]; Chockalingam *et al.* [131]) Hatching space (Chockalingam *et al.* [131]) Overcure depth (Chockalingam *et al.* [131])
	Geometrical deformation	Laser speed (i.e. conversion rate) (Corcione *et al.* [135]) Part dimension (Xing *et al.* [132]) Part length (Li *et al.* [133] Hatching space (Salmoria *et al.* [134]) Evaporation heterogeneity (Zhou *et al.* [136])
Surface quality	Roughness	Layer thickness (Zhou *et al.* [130]; Cedorge *et al.* [139]) Overcure depth (Zhou *et al.* [130]) Considered axis (Dikova *et al.* [129]; Xing *et al.* [132]) Suspension optical properties (Dikova *et al.* [129]) Hatching space (Khodaii and Rahini [140]) Surface tilt angle (Khodaii and Rahini [140]; Reeves and Cobb [98])
Microstructure	Porosity	Ceramic solution composition (Johansson *et al.* [137]) Post-processing steps (Chugonov *et al.* [144]) Level of porosity and trapped bonding material (Liu *et al.* [145]; Guessasma *et al.* [146])
Mechanical	Tensile strength	Post-process treatment (Salmoria *et al.* [147])
	Flexural strength	Porosity (Liu *et al.* [145]; Guessasma *et al.* [146]) Sintering temperature (Li *et al.* [133])
	Cracks	Ceramic solution composition (Johansson *et al.* [137]) Residual uncured monomer (Bae and Halloran [149])

Table 9: Proposed VPP property and defect classification according to main VPP works